Jurnal Kejuruteraan 38(4) 2026: 1733-1756
https://doi.org/10.17576/jkukm-2026-38(4)-16

# Adsorptive Removal of Phosphorus from Water Using Raw Lala Clam Shells as Adsorbent: Kinetic, Isotherm and Contour Prediction Studies

Nur Husna Muslim[a*], Noorul Hudai Abdullah[b], Norzainariah Abu Hassan[a,c], Nur Atikah Abdul Salim[d] & Siti Maisarah Rahim[e]

[a]*Faculty of Engineering Technology, Universiti Tun Hussein Onn Malaysia, Hab Pendidikan Tinggi Pagoh, Km 1, Jalan Panchor, 84600 Muar, Johor, MALAYSIA*

[b]*Neo Environmental Technology, Centre for Diploma Studies, Universiti Tun Hussein Onn Malaysia, Pagoh Education Hub, 84600 Pagoh, Johor, MALAYSIA*

[c]*Department of Civil Engineering, Politeknik Melaka, No. 2, Jalan PPM10, Plaza Pandan Malim 75250 Melaka, Malaysia Faculty of Engineering & Built Environment, Universiti Kebangsaan Malaysia, MALAYSIA*

[d]*Affiliation School of Occupational, Safety & Health, Netherlands Maritime University College, Johor Bahru, Johor, 80000, MALAYSIA*

[e]*Pejabat Pengurusan Makmal Kampus Cawangan Pagoh, Universiti Tun Hussein Onn Malaysia, Pagoh Education Hub, 84600 Pagoh, Johor, MALAYSIA*

[*]*Corresponding author: nurhusnabintimuslim@gmail.com*

*Received 21 May 2025, Received in revised form 2 March 2026*
*Accepted 2 April 2026, Available online 30 July 2026*

ABSTRACT

*Phosphorus is a major contributor to water pollution, causing harmful algal blooms, oxygen depletion, hence eutrophication. Studies have shown that seashells can effectively remove phosphorus from water due to their calcium carbonate content. While seafood is widely consumed, the shells are typically discarded as waste. Previous studies have explored the use of seashells for phosphorus removal, but none have focused on using raw Lala clam shells. Hence, this study addresses this gap by exploring the potential of Lala clam shells as an adsorbent for phosphorus removal from water at different dosages (2g, 4g, 6g, 8g and 10 g). The adsorbents were characterized using XRD, SEM, EDXRF and FTIR analyses. Batch adsorption experiments assessed the effects of adsorbent mass and contact time on phosphorus removal efficiency. Kinetic analysis revealed that the pseudo-second order model best described the adsorption kinetics ($R^2$ = 0.9964), indicating that the adsorption followed a chemisorption mechanism. Isotherm analysis showed that, although all models had low correlation coefficients, the Langmuir model provided a relatively better fit ($R^2$ = 0.0122), suggesting that phosphorus adsorption occurred on a homogeneous surface, forming a monolayer of phosphorus molecules. The raw Lala clam shells could remove up to 64.2 % of phosphorus with the highest adsorption capacity of 0.0818 mg/g observed at 8 g adsorbent mass. Overall, these findings confirm that raw Lala clam shells exhibit moderate phosphorus removal performance and demonstrate potential as a low-cost and eco-friendly adsorbent, due to their abundance and minimal processing requirements, although further modification is required to improve their adsorption performance.*

*Keywords: Lala clam shell, phosphorus adsorption, batch experiment, kinetic models, isotherm models*

## INTRODUCTION

Untreated wastewater remains a significant global environmental concern due to its continuous discharge into water bodies including lakes, ponds, rivers and oceans (Abdullah et al., 2022; Owhonka et al., 2021). Wastewater is generated from domestic, industrial and agricultural sectors and often contains storm runoff enriched with nutrients, particularly phosphorus (Silva et al., 2023). Excessive phosphorus in water bodies can lead to serious

environmental degradation and water quality deterioration when wastewater is not properly treated (Kesari et al., 2021). At the same time, the demand for high-quality water is rising. Hence, wastewater treatment has become essential (Saleh et al., 2021) to eliminate contaminants, maintain water quality, and ensure the sustainable availability of clean water (Silva et al., 2023).

Phosphorus discharged from untreated or inadequately treated wastewater is the main contributor to nutrient enrichment in water bodies (Li et al., 2021), resulting in serious water quality degradation and leading to eutrophication (Witek-Krowiak et al., 2022). Eutrophication occurs when water bodies accumulate excessive nutrients, particularly phosphorus, which stimulate algal blooms and the overgrowth of aquatic plants. Increased algal biomass reduces sunlight penetration, hence disrupting photosynthesis in submerged plants and altering the balance of aquatic ecosystems. When algae die and decompose, microbial activity consumes dissolved oxygen, creating hypoxic conditions that threaten aquatic life.

While eutrophication can occur naturally, human activities have accelerated its occurrence. The extensive use of phosphorus-based fertilizers in agriculture, along with runoff from farmlands, has enriched water bodies with nutrients, promoting excessive algal growth. Additionally, municipal wastewater contains large amounts of phosphorus from human waste, detergents, and personal care products, which can severely impact the aquatic environment if inadequately treated before discharge (Chae et al., 2021). Since phosphorus cannot be fully recycled within water bodies, it becomes the primary pollutant responsible for driving eutrophication (Yang, 2022). As a result, eutrophication has reduced access to potable water, threatening the sustainable supply of clean water for both humans and ecosystems (Akinnawo, 2023).

In aquatic environments, phosphorus exists in inorganic and organic forms, with inorganic phosphates being the most prevalent in wastewater systems (Witek-Krowiak et al., 2022). Organic phosphorus is commonly present as phosphate esters from biological materials, whereas inorganic phosphorus exists primarily as orthophosphate and polyphosphate (Li et al., 2021). Through biological and chemical degradation processes, both forms are converted into orthophosphate, the most stable form in water bodies and a major contributor to eutrophication (Salim et al., 2021). In agricultural systems, excess phosphates not absorbed by plants are transported into surface waters through leaching and runoff, further increasing phosphorus loads in receiving water bodies (Usman et al., 2022).

Regulations have been established to control phosphorus discharge into surface waters. The United States Environmental Protection Agency (USEPA) mandates a total phosphorus (TP) limit of less than 0.8 mg/L, while the European Union (EU) sets 2 mg/L for populations of 10,000 to 100,000 (Salim et al., 2021). According to the USEPA, phosphate concentrations exceeding 0.025 mg/L can trigger algal blooms due to eutrophication (Usman et al., 2022). Phosphate levels above 1.0 mg/L may disrupt coagulation processes in water treatment plants (Owhonka et al., 2021). In Malaysia, strict phosphorus effluent standards have been implemented, with limits of 5.0 mg/L (Standard A) and 10.0 mg/L (Standard B) to control excess phosphorus in receiving water bodies (Abdullah et al., 2022).

Excessive phosphorus in water can be treated using various methods, including adsorption, biological, and chemical treatments. The biological processes for wastewater treatment such as activated sludge systems or constructed wetlands can effectively remove phosphorus but are often variable due to operational challenges and require careful monitoring. The chemical treatments such as precipitation can achieve rapid phosphorus removal but involve high costs and generate secondary sludge that requires proper disposal. Hence, among these methods, adsorption stands out as a promising technology for phosphorus removal due to its high efficiency, simplicity, ease of operation, and low material costs, making it suitable for sustainable wastewater treatment (Salim et al., 2021).

Calcium carbonate ($CaCO_3$) is well known for its strong affinity toward phosphate ions and has been widely reported as an effective adsorbent for phosphorus removal from wastewater (Abdullah et al., 2022). Raw seashell materials are naturally rich in $CaCO_3$, making them an environmentally sustainable and economical alternative adsorbent (Mokhtera et al., 2023). Accordingly, previous studies have explored the utilization of $CaCO_3$ derived from various seashell wastes, including raw hard clam shell (Abdullah et al., 2025), raw waste marsh clam shell (Abdullah et al., 2024), scallop and whelk shells (Brakemi et al., 2023), as low-cost and sustainable adsorbents for phosphorus removal in aqueous environments. Despite the high consumption of seafood, clam shells are often discarded as waste, representing an underutilized bio-resource with significant potential for environmental applications (Verma et al., 2025).

Previous studies have demonstrated the potential of various seashell wastes as phosphorus adsorbents, focusing on specific shell types, processing conditions, or operational scopes. For instance, Brakemi et al. (2023) investigated scallop and whelk shells, applying response surface methodology (RSM) and Central Composite Design (CCD) to optimize phosphate removal, including kinetic and isotherm modeling, and even testing column performance with real wastewater. Other studies on raw hard clam shells (Abdullah et al., 2025) and raw waste marsh clam shells (Abdullah et al., 2024) primarily focused on batch adsorption experiments, examining pseudo-first and

pseudo-second order kinetic models, and Freundlich and Langmuir isotherms.

The short-neck clam (Orbicul*aria orbiculata*), locally known as the Lala clam, is abundant in Malaysia and Indonesia, generating shell waste with minimal economic value. Lala clam shells comprise approximately 95% $CaCO_3$ (Ahmed Eljiedi et al., 2019) that may enhance their adsorption performance (Singh et al., 2022). Although various seashells have been investigated as phosphorus adsorbents, raw Lala clam shells remain unevaluated. Previous studies mainly focused on batch adsorption experiments with limited kinetic and isotherm modeling, statistical optimization, or predictive tools for practical applications. Therefore, this study represents the first comprehensive investigation of raw Lala clam shells as an adsorbent for phosphorus removal.

This evaluation includes batch adsorption experiments and physicochemical characterization, employing X-ray diffraction (XRD), scanning electron microscopy (SEM), energy-dispersive X-ray fluorescence (EDXRF), and Fourier-transform infrared spectroscopy (FTIR). Adsorption data are validated using kinetic models (pseudo-first order, pseudo-second order, Boyd) and isotherm models (Langmuir, Freundlich, Henry), while a contour prediction diagram is developed to guide practical dosing. By integrating these approaches, this study not only fills a knowledge gap, but also offers a novel, practical, and sustainable strategy for phosphorus removal, providing insights for researchers and practitioners in water treatment field.

Hence, the objectives of this study are (1) to elucidate a physicochemical characterization of raw Lala clam shells as adsorbents, (2) to identify the removal efficiency E (%) and adsorption capacity q (mg/g) of raw Lala clam shells onto phosphorus in aqueous phosphate solution through batch experiment when equilibrium rate is achieved, (3) to assess the kinetic and isotherm adsorption models for raw Lala clam shells adsorbents by removing phosphorus from aqueous phosphate solution through batch experiments, and (4) to evaluate the effectiveness of phosphorus removal with the required mass of adsorbents at various initial concentrations by implementing the contour prediction diagram.

## METHODOLOGY

### ADSORBENTS

Lala clam shells were used in this study as adsorbents that sourced from Rengit, Johor, Malaysia. The raw Lala clam shells were first cleaned by using tap water. The cleaned shells were then rinsed using deionized water before drying them under the sunshine. Then, the shells were dried in an oven at 30 °C for 2 days before going through the crushing process. The crushed shells were sieved by using a sieve with a particle size range of 1.18 mm to 2.36 mm. After that, the sieved shells were weighed using analytical balance and divided into 2, 4g, 6g, 8g and 10 g of raw adsorbents.

### AQUEOUS SOLUTION

The aqueous solutions of 5, 10, 15, 20 and 25 mg/L $PO_4$ were prepared by first preparing a 100 mg/L $PO_4$ solution. Approximately 0.1433 g of $KH_2PO_4$ powder was dissolved in deionized water before being added to 1 L of deionized water. The solution was put in a volumetric flask before being inverted several times to dissolve the powder.

Next, the 50 mg/L of $PO_4$ solution was prepared by taking out approximately 200 mL from the 100 mg/L $PO_4$ solution and diluted with 800 mL of deionized water in a volumetric flask. The flask containing the solution was then inverted many times to ensure the solution was homogenized. From the 1 L of 50 mg/L $PO_4$, the $PO_4$ solutions with the concentration of 5, 10, 15, 20 and 25 mg/L of $PO_4$ were prepared.

### ANALYTICAL METHODS

Each sample was analyzed using DR1900 to ensure that the final phosphorus concentration ranges within ±1 mg/L by using the amino acid method. Additionally, the physicochemical properties of each sample were identified by implementing various methods, including X-ray diffraction (XRD), energy dispersive X-ray fluorescence (EDXRF), scanning electron microscopy (SEM) and Fourier transform infrared spectroscopy (FTIR) analyses.

XRD analysis was conducted at the Material Physics Laboratory, Universiti Tun Hussein Onn Malaysia (UTHM), Pagoh Campus, to determine the crytallographic phases and the crystallinity of inorganic substances (Massit et al., 2021; Abdullah et al., 2023) in the raw Lala clam shell adsorbents. This was achieved by analyzing the diffraction pattern produced when X-rays interact with crystal lattice (Ali et al., 2022) since XRD can detect any new phases formed due to chemical interactions during the phosphorus adsorption (Zhang et al., 2021). The raw Lala clam shell adsorbents were prepared in two separate samples, before and after phosphorus adsorption. The samples were then finely crushed into a powder-like consistency with a minimum of 3 g for each sample before being placed at the center of a circular XRD sample holder. The surfaces were leveled and compacted using a glass plate, ensuring it was evenly spread without any gaps or air. The excess powders around the sample holder edges

were cleaned. Afterward, the samples were analyzed using the Bruker D2 PHASER model. The results were further analyzed using HighScore software at Microelectronics and Nanotechnology-Shamsuddin Research Centre (MiNT-SRC), UTHM (Main Campus) to obtain the final XRD diffraction pattern.

The SEM and EDXRF analyses were conducted at the Nanotechnology Physics Laboratory, UTHM Pagoh Campus, to determine the surface morphology and elemental compositions, respectively, of raw Lala clam shell before and after phosphorus adsorption. The samples (before and after phosphorus adsorption) were dried in an oven at 30 °C for 24 h to remove any residual moisture. After 24 h, the samples were taken out before being placed onto the carbon tapes attached to the SEM specimen stubs, ensuring full coverage of the stub and proper adhesion. The SEM specimen stubs were first wiped with acetone to remove any contaminants before applying the carbon tape. Then, the samples were cleaned using an air blower to remove any loose particles before coated with gold (Au) layer using the Quorum Q150RS sputter coater to enhance conductivity. Afterward, the samples were analyzed using the COXEM EM-30AX PLUS SEM for both analyses, where SEM was used to examine surface morphology while EDXRF determined elemental composition.

FTIR analysis was conducted at the Analytical Laboratory, UTHM Pagoh Campus, to examine the chemical composition and the presence of chemical bonds (Abdullah et al., 2023) in raw Lala clam shell adsorbents. The samples of before and after phosphorus adsorption, were prepared and finely ground into powder. The attenuated total reflectance (ATR) crystal sampling surface of the Cary 630 FTIR model was wiped with ethanol to prevent contamination. The first sample was placed on the ATR sampling surface, and the frequency range was set from 600 cm $^{-1}$ to 4000 cm $^{-1}$ to obtain its IR spectrum. The procedure was then repeated for the next sample. The first sample was carefully removed, and the ATR sampling surface was cleaned again with ethanol before introducing the next sample. This process ensured reliable and consistent spectral data for further analysis. Hence, the IR spectrum for both samples was obtained.

## BATCH EXPERIMENTS

Two sets of batch experiments were performed in this study. The first batch aimed to evaluate the effectiveness of phosphorus removal with the required adsorbent masses at various initial concentrations by implementing a contour prediction diagram. In this batch experiment, raw adsorbents with masses of 2, 4, 6, 8 and 10 g were added into separate conical flasks containing 100 mL of aqueous phosphate solutions with initial phosphorus concentrations of 5, 10, 15, 20 and 25 mg/L respectively. Each sample was shaken together at 170 rpm for 4320 min using an orbital shaker to ensure the equilibrium was reached. After 4320 min, the raw adsorbents were separated from the solutions to obtain the adsorbent and the solution samples. The pH level of each sample was recorded before the suspended adsorbents in the solutions were filtered using a vacuum pump. Then, the final phosphorus concentration in the aqueous solution for each sample was determined using the amino acid method.

The second batch experiment was conducted to determine the removal efficiency E (%) and adsorption capacity q (mg/g), and to evaluate the kinetic and isotherm adsorption models of Lala clam shells adsorbents for phosphorus removal from aqueous phosphate solution. This batch experiment used a fixed initial concentration of 10 mg/L of aqueous solution. The raw adsorbents with masses of 2, 4, 6, 8 and 10 g were dissolved in different conical flasks containing 100 mL of 10 mg/L aqueous solution. Each sample was agitated until equilibrium was reached at 170 rpm for 30, 120, 300, 1440 and 4320 min. Following equilibrium, the samples were then filtered and analyzed using the same procedure as in the first batch.

## ANALYSIS OF KINETIC MODEL

The pseudo-first-order (PFO) and pseudo-second-order (PSO) models were applied in the kinetic analysis to determine the adsorption mechanism (Salim et al., 2021) and the adsorption kinetics (Abdullah et al., 2022) of phosphorus onto adsorbents. Additionally, the Boyd kinetic model was also utilized.

## PSEUDO-FIRST ORDER MODEL

The main concept of pseudo-first order model is the total rate of the unoccupied sites relative to the occupied sorption sites, which is essential in analyzing the validity of linear and nonlinear forms (Abdullah et al., 2023). This model can be represented as equation (1).

$$\ln(q_e - q_t) = \ln(q_e) - k_1 t_i \quad (1)$$

The exponents $q_t$ (mg/g) and $q_e$ (mg/g) represent the amount of solute (phosphorus) adsorbed per unit mass of adsorbent at any given time, and at equilibrium, respectively, while $k_1$ is the rate constant of the pseudo-first order model.

## PSEUDO-SECOND ORDER MODEL

The pseudo-second order model predicts that the available sites on the adsorbent are proportional to the total amount

of solute adsorbed (Abdullah et al., 2023). The adsorption rate correlates with the solute concentration on the surface of the adsorbent. The pseudo-second order model is expressed in equation (2).

$$\frac{t}{q_t} = \frac{1}{k_2 q_e{}^2} + \frac{t}{q_e} \quad (2)$$

Where, the $q_t$ (mg/g) and $q_e$ (mg/g) represent the phosphorus concentration adsorbed, at any time t and at equilibrium, respectively, while $k_2$ is the rate constant of pseudo-second order, which may be analyzed by plotting $\frac{t}{q}$ against $t_i$.

## BOYD KINETIC MODEL

Benjelloun et al. (2021) identified a Boyd model as one of the key kinetic models for distinguishing the diffusion of intraparticle and extraparticle. Hence, Boyd's kinetic model is expressed in equation (3).

$$B_t = -0.4977 - \ln\left(1 - \frac{Q_t}{Q_e}\right) \quad (3)$$

Where, $B_t$ is the constant value of Boyd, $Q_t$ represents the adsorbate value in adsorbent at time t (mg/g) and $Q_e$ expresses the adsorbate value in adsorbent at equilibrium condition (mg/g). To examine this model, it is essential to convey the $B_t$ in a graph form as a measure of contact time t and determine the coefficient of determination $R^2$.

## ANALYSIS OF ISOTHERM MODEL

Freundlich, Langmuir (Salim et al., 2021) and Henry (Ehiomogue et al., 2021) models were used for the isotherm analysis to determine the adsorption isotherm of phosphorus onto adsorbents (Abdullah et al., 2022). The removal efficiency percentage (E) and adsorption capacity (q) were identified using equations (4) and (5).

$$E = \frac{(C_i - C_f)}{C_i} \times 100\% \quad (4)$$

$$q = \frac{(C_i - C_f) \times V}{m} \quad (5)$$

Where $C_i$ is the concentration value at the initial, $C_f$ is the concentration value at the final, *m* represents the mass of adsorbents, and *V* expresses the volume.

## FREUNDLICH MODEL

The adsorbate and the adsorbent surface that bind physically cause the Freundlich adsorption to occur (Ikhsan et al., 2022). Theoretically, Freundlich predicts that the occurrence of adsorption is in heterogeneous layers and multilayers. Freundlich model shows the difference on a surface and the increase of active sites (Li et al., 2021), which is expressed in equation (6).

$$\ln q_e = \ln K_F + \frac{1}{n} \ln C_e \quad (6)$$

Where, the exponent of $q_e$ is the absorbed metal ion concentration when it reaches equilibrium (mg/g), *Ce* is the concentration of solution containing metal ions at equilibrium (mg/L), while $K_F$ and $\frac{1}{n}$ are the rate constants of the Freundlich model.

## LANGMUIR MODEL

The reaction of chemical bonds between the absorbent and adsorbate surfaces causes the occurrence of Langmuir isotherm (Ikhsan et al., 2022). Langmuir's model predicted the adsorbent to be saturated when the coverage of monolayer adsorbate on the adsorbent was connected to a homogeneous surface without the reactions from absorbed molecules (Salim et al., 2021). The equation of this model was expressed in equation (7),

$$\frac{1}{q_e} = \frac{1}{K_L q_{max} C_e} + \frac{1}{q_{max}} \quad (7)$$

Where Langmuir is represented by $K_L$ is the energies of interaction and $q_{max}$ is the maximum of adsorption capacity.

## HENRY'S ISOTHERM MODEL

This model is a one-parameter isotherm that defines adsorption equilibrium at low and constant temperatures. The adsorbate equilibrium in a fluid is associated with the adsorptive fluid partial pressure. This situation is expressed in equation (8).

$$Q_e = K_H C_e \quad (8)$$

$Q_e$ is the amount of adsorbate at the equilibrium condition (mg/g), $K_H$ is the value of constant and $C_e$ is the adsorbate concentration on the adsorbent at equilibrium.

# RESULTS AND DISCUSSION

## PHYSICOCHEMICAL CHARACTERISTICS OF RAW LALA CLAM SHELL

### XRD ANALYSIS

XRD analysis was performed to identify the crystallographic phases of synthesized materials (Massit et al., 2021) and to determine the purity of inorganic substances (Abdullah et al., 2023) in raw Lala clam shell adsorbents before and after phosphorus adsorption. Figure 1 depicts the quantification and XRD patterns for raw Lala clam shells before and after phosphorus adsorption.

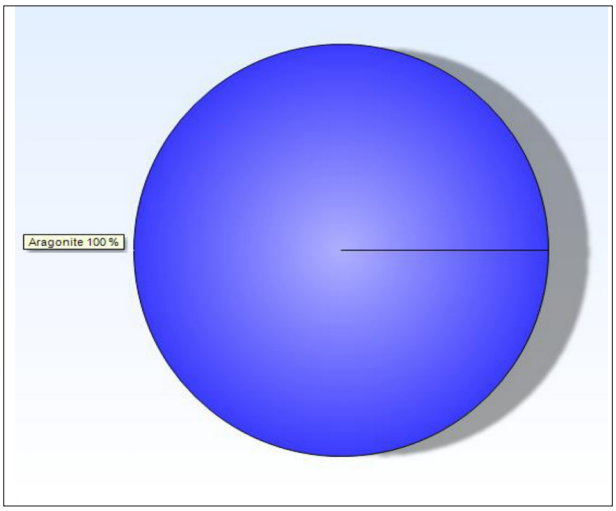


(a)

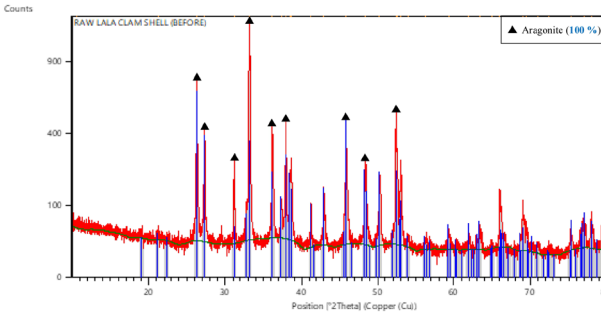


(b)

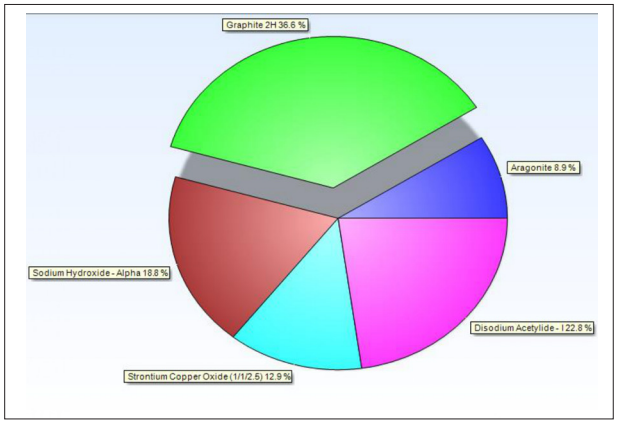


(c)

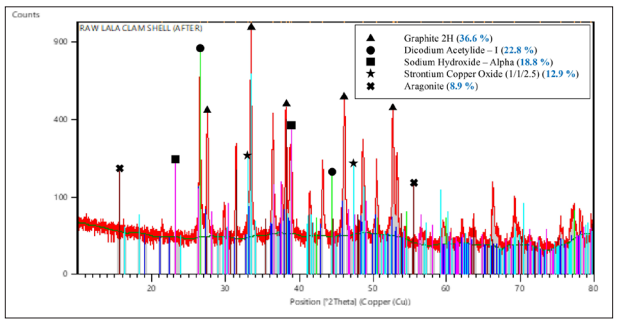


(d)

FIGURE 1. (a) The quantification before adsorption and (b) XRD patterns before adsorption, (c) The quantification after adsorption, and (d) XRD patterns after adsorption of raw Lala clam shell-based adsorbents

Based on Figures 1(a) and 1(b), aragonite is the primary component identified in the XRD pattern of raw Lala clam shells, consistent with previous studies on various shell-based adsorbents. Nayeem et al. (2023) reported that cockle shell powder primarily consists of aragonite. Similarly, Abdullah et al. (2023b) confirmed that aragonite and calcium carbonate are the major components in raw marsh clam shells, contributing to their effectiveness in phosphorus adsorption. Hamid (2022) states that aragonite is a crystal form of calcium carbonate ($CaCO_3$) that naturally occurs in marine organisms' shells, such as clams. It is a primary mineral in clam shells since its structure is stable (Habte et al., 2020). Hence, raw Lala clam shells consist of 100 % aragonite before going through phosphorus adsorption (Nhung et al., 2023).

After phosphorus adsorption, the XRD patterns show peaks that the HighScore software automatically assigned to graphite-2H, dicodium acetylide-I ($Na_2C_2$), sodium hydroxide-alpha (NaOH), and strontium copper oxide (1/1/2.5) ($SrCuO_3$), as shown in Figures 1(c) and 1(d). While these peaks appear in the analysis, the formation of such compounds is not chemically plausible in a $CaCO_3$–phosphate aqueous system and likely results from trace contamination. Aragonite remains the dominant crystalline phase, and observed changes in diffraction intensity are consistent with phosphorus adsorption on the surface of raw Lala clam shells (Brandão et al., 2021). Brakemi et al. (2023) reported peak shifts, decreased peak intensity, and the disappearance of specific diffraction peaks after adsorption. These changes were indicative of phosphorus adsorption onto the surface of adsorbents.

Interestingly, phosphorus was not detected in the XRD analysis after adsorption, possibly due to the detection limits of the XRD equipment. A similar observation was reported by Santos et al. (2024), who found that phosphorus was not detected after adsorption onto biogenic calcium carbonate. The study suggested that the phosphorus may exist as an amorphous surface precipitate or in a dispersed phase, making it undetectable by XRD. This phenomenon occurs due to the reaction of phosphorus with calcium, forming small and highly dispersed calcium phosphate particles on the $CaCO_3$ surface. If these particles are amorphous or extremely fine, they may not generate distinct diffraction peaks, making them difficult for XRD to detect (Santos et al., 2024).

Graphite-2H was observed at 36.6 % in raw Lala clam shells after phosphorus adsorption. It is a form of carbon with a hexagonal crystal structure (Albetran, 2020). According to Piaskowski & Zarzycki (2020), the detection of graphite in raw Lala clam shells after phosphorus adsorption can result from carbonaceous contamination during the adsorption process. Furthermore, disodium acetylide-I, a compound of sodium and carbon, was detected at 22.8% (Swapna & Sankararaman, 2020). The presence of these phases is not chemically expected in a $CaCO_3$–phosphate system and may reflect trace contamination.

Sodium hydroxide-alpha, identified at 18.8% in raw Lala clam shells after phosphorus adsorption, is a crystalline solid in an alkaline compound (Kljajević et al., 2022). Similarly, Strontium copper oxide (1/1/2.5) detected as a complex oxide compound comprised of strontium and copper (Khalil et al., 2022). However, their presences in phosphorus adsorption onto raw Lala clam shells could be due to impurities containing this compound (Bashir et al., 2023). The main crystalline phase remains aragonite, and the reduction proves that raw Lala clam shells were transformed under chemical interactions (Li et al., 2020).

## SEM ANALYSIS

SEM analysis was conducted to identify the surface morphology (Abdullah et al., 2023) of raw Lala clam shells before and after phosphorus adsorption. The study was performed at a magnification of 2,000× with a scale bar of 10 μm for both adsorbents. These settings ensure that the images focus on the microscopic structures within an excellent scale (Zheng et al., 2024). Figures 2(a) and 2(b) depict the surface morphology of raw Lala clam shells before and after phosphorus adsorption at 2,000× magnification and 10 μm scale bar.

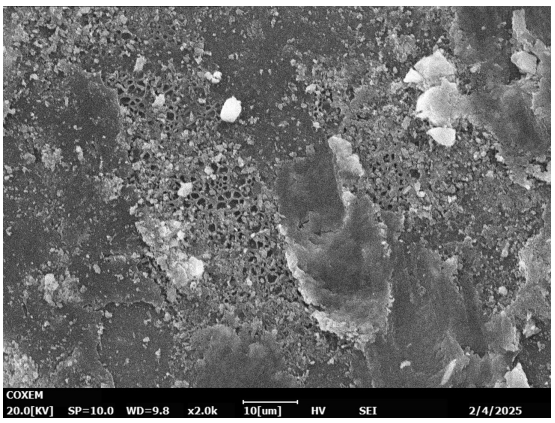


(a)

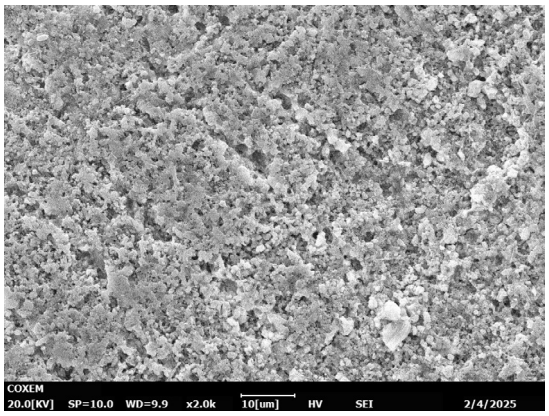


(b)

FIGURE 2. SEM photomicrographs for raw Lala clam shells (a) before and (b) after phosphorus adsorption, showing surface characteristics at a magnification of 2,000×

Figure 2(a) shows the raw Lala clam shell adsorbent before phosphorus adsorption. It demonstrates a porous structure with interconnected voids of varying sizes (Singh et al., 2025). The high porosity increases the surface area of raw Lala clam shell adsorbent, which is essential for efficient adsorption (Lee et al., 2021). Similar porous structures have been reported in other shell-based adsorbents, including marsh clam shells (Abdullah et al.,

2023b) at 10,000× magnifications, exhibiting an irregular, rough, and porous surface. The raw Lala clam shell adsorbent surface also contains small cracks and fractures, which enhance accessibility to adsorption sites (María Lorena et al., 2025). Additionally, the texture appears rough and uneven, with jagged and fragmented regions (Muchunku et al., 2023; Cao et al., 2025). The presence of bright and dark contrasts in the image suggests differences in elemental composition, where brighter areas describe heavier elements, including calcium, while darker regions represent organic matter or voids (Rebora et al., 2023; Kazak et al., 2021).

Following phosphorus adsorption, as seen in Figure 2(b), the SEM image shows a significant reduction in porosity, with many previously visible voids appearing filled or blocked (Chen et al., 2022). This is consistent with the findings of Brakemi et al. (2023), who reported that scallop and whelk shells exhibited smoother surfaces after phosphorus adsorption, indicating phosphorus attachment. Additionally, the surface appears denser and more compact in raw Lala clam shell adsorbent, suggesting phosphate ions have successfully attached to the shell structure (Shao et al., 2022). Compared to the state before phosphorus adsorption, the texture looks smoother and more homogeneous, with fewer cracks and irregular regions (Benaoune et al., 2025; Shi et al., 2023). The disappearance of small cracks and fractures describes structural changes caused by interactions between phosphate ions and the adsorbent (Moustafa et al., 2024). Additionally, increased particle aggregation forms a compact structure, which might be attributed to phosphorus bonding with calcium-rich components, leading to flocculation (Adly et al., 2022; Gonçalves et al., 2024). The brighter spots in the SEM image are more prominent after adsorption, indicating phosphorus deposition on the shell surface.

## EDXRF ANALYSIS

EDXRF analysis was conducted to identify the elemental compositions of raw Lala clam shells before and after phosphorus (Abdullah et al., 2022). Hence, the results of this analysis help in understanding the compositional changes in raw Lala clam shells caused by phosphorus adsorption (Kaljunen et al., 2022). Figures 3(a) and 3(b) depict the elemental compositions of the adsorbents before and after adsorption, respectively.

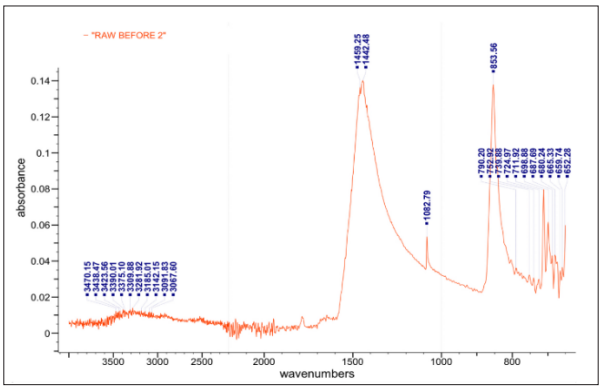


(a)

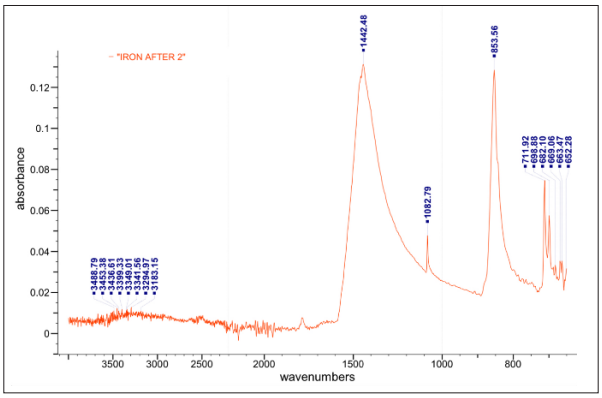


(b)

FIGURE 3. Elemental compositions presence of raw Lala clam shells (a) before and (b) after phosphorus adsorption

Based on Figure 3, the differences in elemental composition between before and after phosphorus adsorption onto raw Lala clam shells indicate potential phosphorus adsorption onto the shell surface. These variations are further analyzed (Table 1) to understand the elemental composition differences before and after phosphorus adsorption.

TABLE 1. Elemental compositions of raw Lala clam shells before and after phosphorus adsorption

| Element | Raw Lala clam shells before phosphorus adsorption (%) | Raw Lala clam shells after phosphorus adsorption (%) |
|---|---|---|
| Ca | 6.76 | 44.22 |
| Si | 5.01 | - |
| O | 40.46 | 44.82 |
| Fe | 6.16 | - |
| S | 1.83 | - |
| Al | 3.18 | 0.31 |
| Sr | 0.18 | 0.15 |
| Na | 0.56 | 0.14 |
| Mg | 0.49 | 0.34 |
| C | 35.37 | - |
| K | - | 0.13 |
| Cu | - | 1.53 |
| Total | 100.00 | 100.00 |

Based on Table 1, the percentage of calcium (Ca) element in raw Lala clam shells increased from 6.76% to 44.22% after phosphorus adsorption. This finding contrasts with a study by Muslim et al. (2025), where calcium content in marsh clam shells decreased from 72.86% to 49.95% after phosphorus adsorption. According to Mititelu et al. (2021), calcium is the primary composition in clam shells, generally in the calcium carbonate ($CaCO_3$) form. Therefore, the very low initial calcium value and the sharp increase observed after adsorption in this study are more likely due to normalization artefacts or sample heterogeneity, rather than absolute calcium enrichment or depletion. (Pervov et al., 2022). In contrast, the reduction in calcium content reported by Muslim et al. (2025) is more consistent with the phosphate adsorption mechanism involving calcium dissolution.

Silicon (Si) element was also detected at 5.01% before phosphorus adsorption but became undetectable after adsorption. This element likely originated from environmental contamination or habitat exposure, including sand or silicates (Pikula et al., 2020). The element was undetectable after the phosphorus adsorption process due to the dissolution of the silicates (Li et al., 2022). However, silicon was not reported in the previous study of marsh clam shells, indicating a possible difference in the initial composition of the adsorbent material used.

In addition, the oxygen (O) increase from 40.46% to 44.82% proves that new oxide phases occurred during the phosphorus adsorption process (Deng et al., 2020). This element in raw Lala clam shells is a part of mineral and organic matter (Ubaldini et al., 2024), where it may be present in calcium carbonate ($CaCO_3$) compounds (Yadav et al., 2021). However, Muslim et al. (2025) did not report oxygen content before or after adsorption, making direct comparisons difficult. This omission could be due to differences in data presentation, as some studies focus on major and trace elements rather than non-metallic components like oxygen.

The iron (Fe) content in raw Lala clam shells was 6.16% before adsorption but became undetectable after the process. This suggests that iron might have been removed through a leaching mechanism due to its solubility in the adsorption environment (Van et al., 2020). In contrast, Muslim et al. (2025) reported a decrease in iron from 2.02% to 1.48% after adsorption rather than complete removal. The variation could result from differences in the initial iron composition or the adsorption conditions. According to Longhini et al. (2021), iron in clam shells often originates from environmental contamination, such as iron oxides in sediments.

The aluminum (Al) in raw Lala clam shells decreased from 3.18% to 0.31% after phosphorus adsorption, indicating a significant reduction. Muslim et al. (2025) also observed a decrease in aluminium content, from 1.39% to 0.24%, aligning with this study's findings. The reduction suggests that aluminum may have been partially dissolved or removed during the adsorption process. Normally, aluminum in shells can originate from environmental exposure and can be affected by adsorption conditions (Schöne et al., 2023).

Sulfur (S) was present at 1.83% before adsorption but became undetectable after the process. In contrast, strontium (Sr), sodium (Na) and magnesium (Mg) showed slight decreases from 0.18% to 0.15%, 0.56% to 0.14%, and 0.49% to 0.34%, respectively. These elements could be environmental contaminants present in the raw Lala clam shells or naturally embedded in the shell structure (Schöne et al., 2023), while sulfur typically exists in organic compounds or sulfates (Zhang et al., 2022). These reductions or disappearance suggest that the elements were either leached out or structurally altered during adsorption (Van et al., 2020). Muslim et al. (2025) did not report values for S, Sr, Na, or Mg, which prevents a direct comparison.

Similarly, carbon (C) was initially present at 35.37% in raw Lala clam shells but became undetectable after phosphorus adsorption. This could be attributed to the release of carbon as carbon dioxide ($CO_2$) during chemical

processing (Park et al., 2022). In comparison, Muslim et al. (2025) reported an increase in carbon content, from 23.73% to 48.33% after phosphorus adsorption. It may be due to the adsorption of organic phosphate compounds or the deposition of carbon-containing species onto the shell surface. The discrepancy may be due to differences in the adsorption environment, materials used, or the presence of other compounds influencing carbon retention. According to Azarian & Sutapun (2022), carbon is a key component of calcium carbonate ($CaCO_3$) that makes up the shells.

Finally, potassium (K) and copper (Cu) were only detected after phosphorus adsorption, at 0.13% and 1.53%, respectively. The presence of potassium after adsorption may be due to ion exchange between potassium ions in the solution and calcium ions from the clam shell matrix, as potassium is commonly found in marine environments and can be introduced through the adsorption process (Li et al., 2021). Copper, on the other hand, may have originated from external contamination, such as leaching from experimental equipment or reagents used during the adsorption process (Tian et al., 2021). The previous study by Muslim et al. (2025) did not mention these elements, suggesting either their absence in the marsh clam shells studied or that differences in experimental conditions influenced their detection.

## FTIR ANALYSIS

FTIR analysis was conducted to analyze the chemical composition and the functional groups or chemical bonds that existed (Abdullah et al., 2023) in raw Lala clam shells before and after phosphorus adsorption. Figures 4(a) and 4(b) depict the results from FTIR analysis for raw Lala clam shells before and after phosphorus adsorption, respectively.

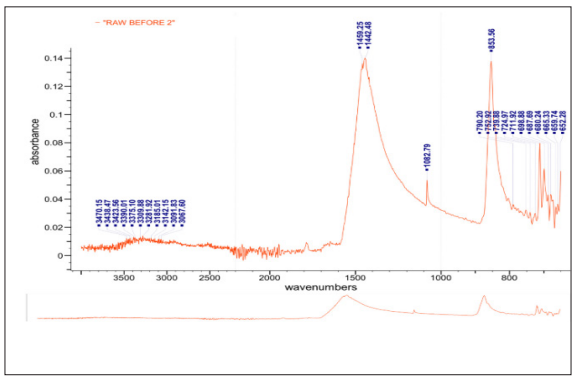


(a)

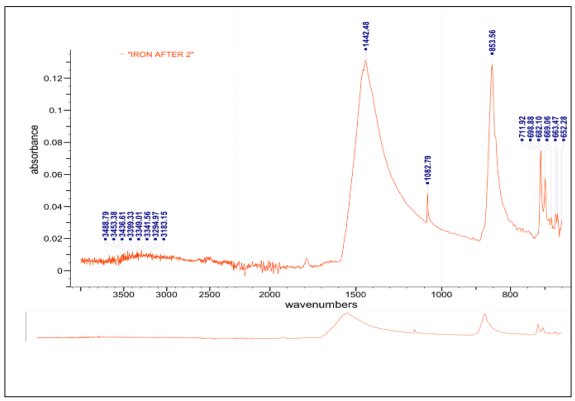


(b)

FIGURE 4. FTIR results for raw Lala clam shells (a) before and (b) after phosphorus adsorption

Based on Figure 4, FTIR analysis was performed within the frequency range from 600 $cm^{-1}$ to 4000 $cm^{-1}$, before and after phosphorus adsorption onto raw Lala clam shells. The increase or decrease in wavenumber after phosphorus adsorption suggests changes in bond environments due to interaction with phosphorus molecules, altering the energy required for bond stretching (Ganta et al., 2021). The interpreted IR spectrum of raw Lala clam shells, before and after adsorption, is shown in Table 2 to observe the frequency differences and identify the detected functional group.

Based on Table 2, the hydroxyl (OH) group was dominantly observed in raw Lala clam shells both before and after phosphorus adsorption at the frequency of 3419.83 $cm^{-1}$, 3423.56 $cm^{-1}$, 3438.47 $cm^{-1}$ and 3470.15 $cm^{-1}$ (Salim et al., 2021). This aligns with findings from a previous study by Nayeem et al. (2023), who observed a weak OH band at 3640 $cm^{-1}$ in cockle shells due to low moisture content. After phosphorus adsorption, their study noted sharper OH bands, indicating a reaction between calcium oxide (CaO) and water. Similarly, the presence of these hydroxyl groups in this study on raw Lala clam shells can be attributed to the partial hydration of calcium carbonate ($CaCO_3$), primarily in the form of aragonite (Sheng et al., 2023). The stretching vibration of OH was observed in the range of 3259.6 $cm^{-1}$ to 3390.01 $cm^{-1}$ in this study of raw Lala clam shell, indicating that the dominant functional group was alcohols (Ali et al., 2024). The broadness of the OH group is due to hydrogen bonding since it involves a strong hydrogen bond, requiring a significant amount of energy to stretch (Medel & Suhm, 2021).

The functional group detected at 3142.15 $cm^{-1}$, 3185.01 $cm^{-1}$ and 3196.19 $cm^{-1}$ in raw Lala clam shells correspond to nitrogen-hydrogen (NH) stretching, indicative of amides or amine groups. This presence likely originates from protein residues within the calcified shell structure, where embedded proteins contribute amine (–$NH_2$) or amide (–$CONH_2$) groups (Verma et al., 2022). The interactions with phosphorus compounds can further influence NH stretching frequencies by forming weak hydrogen bonds that cause slight spectral shifts (Ai et al., 2023). As NH bonds require less energy to stretch than OH bonds, they appear at lower frequencies (Zojaji et al., 2021). Variations in NH stretching frequencies after phosphorus adsorption suggest that nitrogen-containing functional groups participate in phosphorus interactions, reinforcing the role of amides or amines in the adsorption process (Zojaji et al., 2021).

The absorption band at 3091.83 $cm^{-1}$ corresponds to the C=C–H asymmetric stretching vibration, indicating the presence of alkenes group in raw Lala clam shells. This vibration is more likely associated with carbonate-related functional groups or surface-bound phosphate species rather than organic unsaturated compounds, given that raw Lala clam shells are predominantly composed of calcium carbonate. Minor contaminants, including trace amounts of organic pollutants or lipids, may also be responsible for these bands (Sun et al., 2023). The C=C stretching vibration, when bonded with hydrogen (H), generally requires slightly lower energy, suggesting limited involvement in adsorption interactions (Mohan et al., 2020). Additionally, the IR spectrum showed a CH stretching vibration at 3067.60 $cm^{-1}$, suggesting the presence of hydrogen atoms, indicating the existence of benzene-like compounds in the shell matrix (Chruszcz-Lipska et al., 2024).

TABLE 2. Processed IR spectrum of raw Lala clam shells before and after phosphorus adsorption

| Before adsorption | After adsorption | Difference | Detection of functional group | Reference |
|---|---|---|---|---|
| 3470.15 | - | - | O–H | Salim et al. (2021) |
| 3438.47 | - | - | O–H | Salim et al. (2021) |
| 3423.56 | 3419.83 | -3.73 | O–H | Salim et al. (2021) |
| 3390.01 | 3373.24 | -16.77 | OH stretching | This study |
| 3375.10 | 3337.83 | -37.27 | OH stretching | This study |
| 3309.88 | 3311.74 | 1.86 | OH stretching | This study |
| 3281.92 | 3259.56 | -22.36 | OH stretching | This study |
| 3185.01 | 3196.19 | 11.18 | NH stretching | This study |
| 3142.15 | - | - | NH stretching | This study |
| 3091.83 | - | - | C=C–H Asymmetric Stretch | This study |
| 3067.60 | - | - | CH stretching | This study |
| 1459.25 | - | - | CH bending | This study |
| 1442.48 | 1442.48 | 0.00 | CH bending | This study |
| 1082.79 | 1082.79 | 0.00 | CH bending | This study |
| 853.56 | 853.56 | 0.00 | CH deformation | This study |
| 790.20 | - | - | CH deformation | This study |
| 752.92 | - | - | CH deformation | This study |
| 739.88 | 736.15 | -3.73 | CH deformation | This study |
| 724.97 | - | - | Ring bending | This study |

*continue...*

*...cont.*

| | | | | |
|---|---|---|---|---|
| 711.92 | - | - | Ring bending | This study |
| 698.88 | 698.88 | 0.00 | Ring bending | This study |
| 687.69 | - | - | Ring bending | This study |
| 680.24 | 680.24 | 0.00 | Ring bending, CH | This study |
| 665.33 | 667.19 | 1.86 | Ring bending | This study |
| 659.74 | - | - | Ring bending | This study |
| 652.28 | 654.15 | 1.87 | CH bending | Nandiyanto et al. (2023) |

Meanwhile, in this study of raw Lala clam shells, the changes in peak intensities further support the formation of phosphorus-organic complexes, reinforcing their role in adsorption. This suggests that phosphorus adsorption has significantly influenced the shell's chemical composition (Tong et al., 2024). The strong peaks likely result from the formation of phosphorus-organic complexes, possibly forming phosphate esters or coordination complexes with phenyl groups. The prominence of these peaks (Figure 4) highlights the strong interaction between phosphorus and the organic components of the shell, reinforcing its role in the adsorption process.

The CH bending at 1459.25 $cm^{-1}$, 1442.48 $cm^{-1}$, 1082.79 cm $-^{1}$, 654.15 cm $-^{1}$, and 652.28 cm $-^{1}$, as well as CH deformation at 853.56 cm $-^{1}$, 790.20 cm $-^{1}$, 752.92 cm $-^{1}$, 739.88 cm $-^{1}$, and 736.15 cm $-^{1}$, indicate the existence of benzene-like structures within the shell. Nayeem et al. (2023) also observed an intense band around 858 cm $-^{1}$, attributed to carbonate functional groups, which became more prominent after phosphorus adsorption. Similarly, Brakemi et al. (2023) identified key carbonate peaks at 709 cm $-^{1}$, 707 cm $-^{1}$ and 712 cm $-^{1}$, signifying aragonite and calcite structures. These vibrations may originate from organic residues or environmental contaminants on the shell surface (Shukhairi et al., 2025). Compared to stretching modes, the lower energy of these bending and deformation vibrations results in minimal interaction with phosphorus, further supporting their classification as structurally embedded rather than functionally reactive groups (Gokila & Ayyappan, 2021).

The absorption bands observed at 724.97 cm $-^{1}$, 711.92 cm $-^{1}$, 698.88 cm $-^{1}$, 687.69 cm $-^{1}$, 680.24 cm $-^{1}$, 667.19 cm $-^{1}$, 665.33 cm $-^{1}$ and 659.74 cm $-^{1}$ are assigned to out-of-plane bending vibrations of the carbonate ($CO_3^{2-}$) group, which are characteristic of calcium carbonate–based materials, particularly aragonite. These bands are commonly reported in biogenic $CaCO_3$ shells and are associated with lattice vibrations of the carbonate ion within the crystalline structure. The presence of these bands both before and after phosphorus adsorption indicates that the fundamental $CaCO_3$ crystal framework of the raw Lala clam shells was preserved. Notably, a weak absorption band observed at 680.24 cm $-^{1}$ was detected both before and after phosphorus adsorption and is attributed to CH deformation vibrations associated with minor organic residues naturally present in biogenic calcium carbonate shells.

## REMOVAL EFFICIENCY, E (%) AND ADSORPTION CAPACITY, $Q_E$ (MG/G) OF PHOSPHORUS ONTO RAW LALA CLAM SHELL

Removal efficiency, E (%), is a key parameter in adsorption studies as it indicates the effectiveness of an adsorbent in extracting a particular substance from a solution (Yang et al., 2025). It is determined by calculating the differences between the initial and the final concentrations of the adsorbate in the solution (Masliha et al., 2025). A higher removal efficiency signifies a greater capacity of the adsorbent to capture the target ions, highlighting its potential for wastewater treatment applications (Yang et al., 2025). This study investigated raw Lala clam shells as adsorbents for phosphorus removal from water, focusing on their adsorption efficiency. The findings provide insights into the adsorption behavior over time, demonstrating the capability of raw Lala clam shells to reduce phosphorus concentrations effectively. Figure 5 presents the removal efficiency percentage over time for different adsorbent masses, illustrating the adsorption performance of raw Lala clam shells in this process.

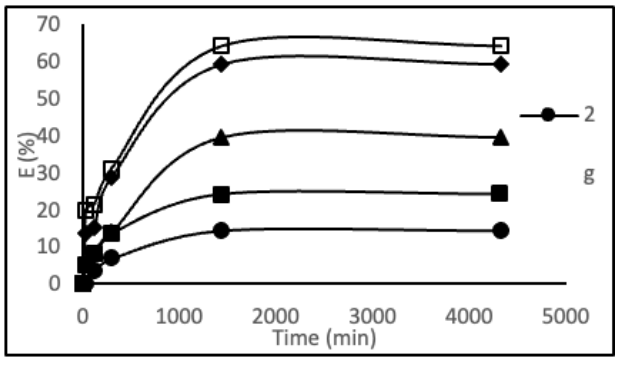


FIGURE 5. Removal efficiency percentage, E (%) against time, t (min) for each mass of adsorbents

Based on Figure 5, the percentage of removal efficiency for every mass of adsorbent increases as time increases. The most excellent removal efficiency for adsorbents with the mass of 2, 4, 6, 8, and 10 g was 14.47%, 24.14%, 39.51%, 59.13%, and 64.20%, respectively, at 1440 min. Beyond this point, the removal efficiency remained constant, with equilibrium reached at 4320 min. The increasing trend in removal efficiency with higher adsorbent mass is attributed to the greater number of available active sites on the raw Lala clam shell's surface, which enhances phosphorus adsorption (Yang et al., 2025). However, as more adsorption sites become occupied, the rate of increase slows down, leading to equilibrium (Wang et al., 2025). The highest removal efficiency of 64.20% at 10 g suggests that adding more adsorbent beyond this point does not significantly improve phosphorus removal. This finding highlights the need to optimize adsorbent mass for efficient and cost-effective phosphorus removal in wastewater treatment.

These findings align with previous studies that investigated the use of various shell-based adsorbents for phosphorus removal. For instance, Nayeem et al. (2023) reported that cockle shell powder achieved up to 52.27% phosphorus removal at an adsorbent concentration of 7 g/L within 40 min, which remained constant. Their study highlighted the role of available binding sites in determining phosphorus removal efficiency, similar to the trend observed in this study. Additionally, Chen et al. (2023) found that raw oyster shell powder exhibited fluctuating phosphate recovery efficiencies, ranging from 79.5% to 97.4% depending on the initial phosphate concentration, which suggests that the nature of the adsorbent and solution conditions significantly affect removal efficiency. Meanwhile, Abdullah et al. (2023a) examined phosphorus removal using ore waste and found that increasing the adsorbent mass enhanced removal efficiency, with values ranging from 29.8% (2 g) to 54.3% (10 g). Their results are comparable to those of this study, where the removal efficiency improved with increased adsorbent mass.

Meanwhile, adsorption is the process of absorbing a material, including ions and molecules, on the surface of an adsorbent (Ikhsan et al., 2022). It is dependent on the interaction of a substance or metal with functional groups in the adsorbent, including the formation of complexes and cation exchange (Svedaite et al., 2025). In this study, the adsorption behavior of phosphorus onto raw Lala clam shells was analyzed by examining the equilibrium adsorption capacity at different adsorbent masses. Understanding these adsorption mechanisms is essential for optimizing the efficiency of phosphorus removal and improving wastewater treatment applications (Usman et al., 2022). Figure 6 depicts the plots of adsorption capacity onto phosphorus for each adsorbent mass.

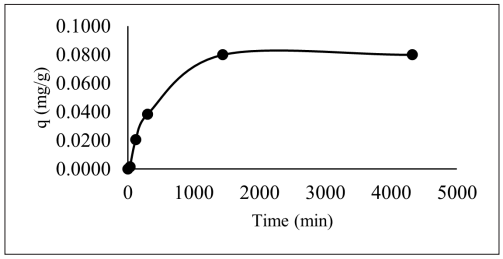


(a)

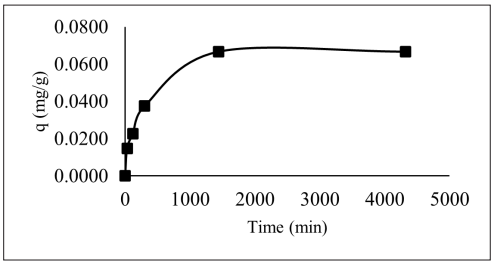


(b)

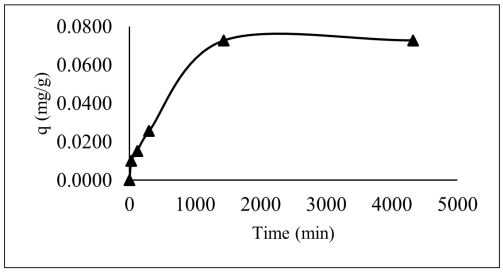


(c)

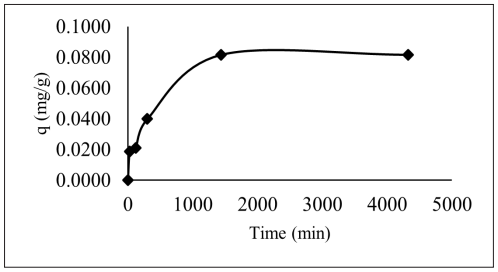


(d)

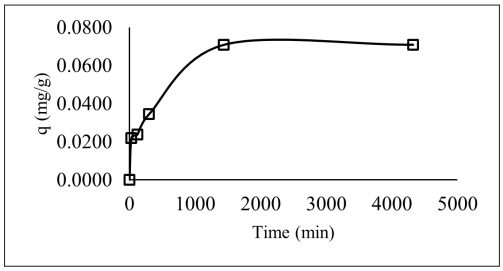


(e)

FIGURE 6. The adsorption capacity with the adsorbent mass of (a) 2 g, (b) 4 g, (c) 6 g, (d) 8 g, and (e) 10 g

Based on Figure 6, each mass of adsorbent reached equilibrium at 1440 min before remaining constant starting from the minute of 4320. Hence, the adsorption capacity for 2, 4, 6, 8, and 10 g of adsorbent mass was 0.0800 mg/g, 0.0668 mg/g, 0.0728 mg/g, 0.0818 mg/g, and 0.0710 mg/g respectively. Initially, increasing the adsorbent mass provides more binding sites, enhancing phosphorus adsorption. However, the adsorption capacity does not increase proportionally at higher adsorbent masses. This is likely due to the saturation of available active sites and the reduced concentration of phosphorus in the solution, which limits further adsorption (Mphahlele et al., 2025). The highest adsorption capacity of 0.0818 mg/g observed at 8 g suggests an optimal adsorbent mass where maximum adsorption occurs before declining slightly at 10 g.

When comparing these results with previous studies, Abdullah et al. (2023a) reported a similar trend using ore waste as an adsorbent where the adsorption capacity decreased at higher adsorbent masses, demonstrating saturation effects. Their study found that adsorption capacities were 0.119 mg/g (2 g), 0.0860 mg/g (4 g), 0.0582 mg/g (6 g), 0.0471 mg/g (8 g) and 0.0434 mg/g (10 g), showing a decline as adsorbent mass increased. In contrast, Nayeem et al. (2023) found that finer cockle shell powder achieved better phosphorus adsorption due to its increased surface area. This indicates that multiple factors influence adsorption performance, including particle size and adsorbent composition.

From these data, although the maximum removal efficiency (64.2%) and the highest adsorption capacity (0.0818 mg/g) obtained in this study are relatively moderate, this level of performance is expected as the Lala clam shells were used in their raw, unmodified form. Nevertheless, the consistent increase in removal efficiency with increasing adsorbent mass and the clear attainment of adsorption equilibrium confirm that phosphorus adsorption effectively occurred. These findings indicate that raw Lala clam shells possess measurable adsorption capability and demonstrate potential for further performance enhancement through surface modification or process optimization, particularly as a low-cost and sustainable adsorbent.

## KINETIC ADSORPTION ONTO RAW LALA CLAM SHELL THROUGH SOLUTIONS

The adsorption kinetic models were implemented using pseudo-first order, pseudo-second order and Boyd kinetic models to identify the adsorption behavior of phosphorus onto raw Lala clam shell. These models were used to predict the adsorption rate (Maimulyanti et al., 2022) and determine the relationship between the contact time and the maximum adsorption capacity (Wu et al., 2021). The $F_e$ and $R^2$ values were computed and compared to identify the best kinetic model by determining the lowest $F_e$ and most excellent $R^2$ (Abdullah et al., 2023). The linear regression kinetic adsorption analysis for the pseudo-first order, pseudo-second order and Boyd kinetic models were generated as depicted in Figures 7(a), 7(b) and 7(c), respectively.

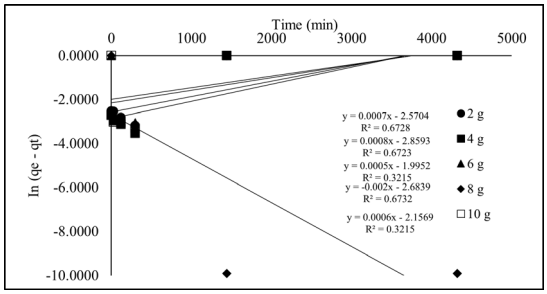


(a)

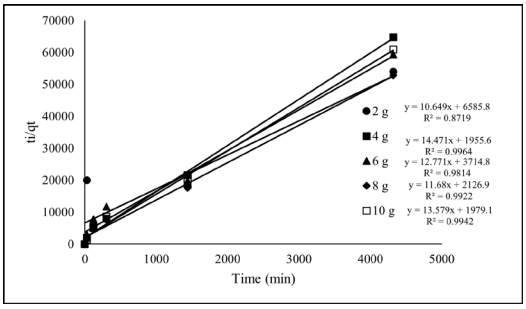


(b)

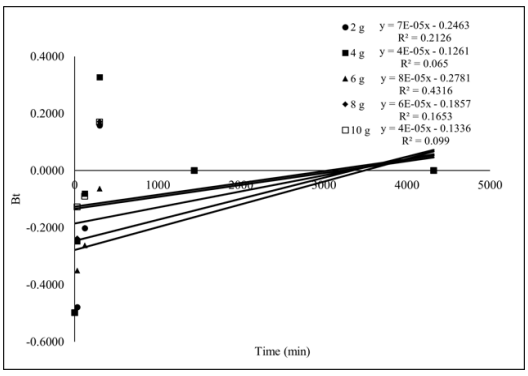


(c)

FIGURE 7. Linear regression analysis for (a) pseudo-first order, (b) pseudo-second order and (c) Boyd kinetic models for the adsorption of phosphorus onto adsorbent from aqueous solution

From Figure 7, Table 3 are generated. Table 3 (a), (b), and (c) indicate the kinetic parameters of pseudo-first order, pseudo-second order and Boyd kinetic models, respectively. Comparing the most excellent $R^2$ and the least $F_e$ values provides insight into the effectiveness of each kinetic model

in describing the adsorption behavior of phosphorus onto raw Lala clam shells. According to Nguyen et al. (2021), an $R^2$ value close to 1 indicates a strong correlation between the data and the model's prediction.

TABLE 3. Parameters of pseudo-first order, pseudo-second order and Boyd kinetic models

(a) Kinetic parameter of pseudo-first order (PFO)

| Mass of adsorbents (g) | $q_{e(theo)}$ (mg/g) | $k_1$ ($min^{-1}$) | $R^2$ | $F_e$ | $q_{e(exp)}$ (mg/g) |
|---|---|---|---|---|---|
| 2 | 0.0765 | -0.0007 | 0.3133 | 3.4498 | 0.0800 |
| 4 | 0.0573 | -0.0008 | 0.6619 | 2.2670 | 0.0668 |
| 6 | 0.1360 | -0.0005 | 0.3215 | 1.6242 | 0.0728 |
| 8 | 0.0683 | -0.0020 | 0.6732 | 387.6864 | 0.0818 |
| 10 | 0.1157 | -0.0006 | 0.3215 | 2.0270 | 0.0710 |

(b) Kinetic parameter of pseudo-second order (PSO)

| Mass of adsorbents (g) | $q_{e(theo)}$ (mg/g) | $k_2$ (min-1) | $R^2$ | $F_e$ | $q_{e(exp)}$ (mg/g) |
|---|---|---|---|---|---|
| 2 | 0.0939 | 0.0172 | 0.8719 | 0.0324 | 0.0800 |
| 4 | 0.0691 | 0.1071 | 0.9964 | 0.1370 | 0.0668 |
| 6 | 0.0783 | 0.0439 | 0.9814 | 0.0325 | 0.0728 |
| 8 | 0.0856 | 0.0641 | 0.9922 | 0.0392 | 0.0818 |
| 10 | 0.0736 | 0.0932 | 0.9942 | 0.0382 | 0.0710 |

(c) Kinetic parameter of Boyd kinetic model

| Mass of adsorbents (g) | $q_e$ (mg/g) | $R^2$ | $F_e$ |
|---|---|---|---|
| 2 | 0.0800 | 0.2126 | 0.3987 |
| 4 | 0.0668 | 0.0650 | 0.7541 |
| 6 | 0.0728 | 0.4316 | 1.0669 |
| 8 | 0.0818 | 0.1653 | 1.7586 |
| 10 | 0.0710 | 0.0990 | 2.0108 |

Table 3(a) shows the pseudo-first order kinetic model data. The highest $R^2$ (0.6732) was observed at 8 g, suggesting that the model statistically fits the trend of adsorption data better at this mass. In contrast, the lowest $R^2$ (0.3133) at 2 g reflects a poor fit, likely due to adsorption at low adsorbent mass being more sensitive to experimental variations and may involve additional kinetic steps not captured by the pseudo-first order model. Despite its higher $R^2$, the $F_e$ at 8 g was the highest (387.6864), indicating that the pseudo-first order model underestimates adsorption, possibly due to complex mechanisms or higher surface interactions at higher adsorbent mass. Conversely, the lowest $F_e$ (1.6242) at 6 g shows the closest agreement between predicted and experimental data, suggesting that the pseudo-first order model is more reliable at intermediate adsorbent masses. These results indicate that the pseudo-first order model provides a rough approximation of equilibrium adsorption but is insufficient to accurately describe the kinetics of phosphorus adsorption onto raw Lala clam shells, particularly at very low (2 g) and high (8 g) adsorbent masses.

Compared to Muslim et al. (2025), the pseudo-first order model was reported to provide the best fit for phosphorus adsorption onto marsh clam shells, with the highest correlation coefficient ($R^2$ = 0.9951), while this study shows a lower $R^2$ range for raw Lala clam shells, indicating a moderate fit. Their study showed that 6 g and 8 g adsorbent masses had similar adsorption capacities, with $R^2$ values of 0.9725 and 0.9951 and $F_e$ values of 0.0288 and 0.0239, respectively. Meanwhile, the 2 g adsorbent mass had slightly lower model fit similar to this study, indicated by $R^2$ = 0.9602 and $F_e$ = 0.0308. In contrast, Abdullah et al. (2023a) found that the pseudo-first order model poorly described phosphorus adsorption when using ore waste as an adsorbent. Their study reported that for an adsorbent mass of 10 g, the pseudo-first order model had a significantly lower $R^2$ value of 0.5242. Additionally, for an adsorbent mass of 8 g, the model showed the lowest $R^2$ value of 0.3885 and the lowest $F_e$ value of 0.9870. These findings indicate that in the case of ore waste, the adsorption process was not well explained by the pseudo-first order model.

Table 3(b) demonstrates that the pseudo-second order model exhibits strong correlation between theoretical and experimental data, suggesting that phosphorus adsorption is mainly governed by chemical interactions rather than physical diffusion (Mohamed et al., 2025). The highest $R^2$ value (0.9964) at 4 g indicates the best kinetic representation, although the same mass recorded the highest $F_e$ value (0.1370), suggesting deviations in adsorption magnitude despite excellent linear correlation. In contrast, the lowest $R^2$ value (0.8719) was observed at 2 g, reflecting a weaker kinetic fit, likely due to limited active sites. Notably, the lowest $F_e$ value (0.0324) also occurred at 2 g, indicating close agreement between predicted and experimental values, despite the lower correlation coefficient. Overall, these results demonstrate that the pseudo-second order model provides a more reliable and robust description of phosphorus adsorption kinetics onto raw Lala clam shells than the pseudo-first order model.

Similarly, Abdullah et al. (2023a) reported that the pseudo-second order model best described phosphorus adsorption onto ore waste, with the highest $R^2$ value of 0.9976 observed at 2 g of adsorbent mass. Their $F_e$ value (0.0097) is the lowest, indicating strong agreement between predicted and experimental data. In contrast, Muslim et al. (2025) found that for phosphorus adsorption onto marsh clam shells, the pseudo-second order model had an $R^2$ value of 0.9889, lower than the pseudo-first order model ($R^2$ = 0.9951). Although the pseudo-second order model exhibited a lower $F_e$ value (0.0154) than the pseudo-first order model (0.0860), the study concluded that the pseudo-first order model more accurately described the overall adsorption kinetics. These findings highlight that the fit of the pseudo-second order model strongly depends on adsorbent type and system characteristics, consistent with this study where the pseudo-second order model provides a better kinetic description than the pseudo-first order model for raw Lala clam shells.

Lastly, Table 3(c) reveals that the Boyd kinetic model does not correlate strongly with the adsorption data, indicating that film diffusion is not the primary rate-controlling step. The highest $R^2$ value (0.4316) was observed at 6 g, but this relatively low correlation still suggests a weaker fit. Conversely, the lowest $R^2$ value (0.0650) occurred at 4 g, suggesting the model poorly captures adsorption kinetics at this mass, likely due to random variations rather than a consistent diffusion mechanism. The lowest $F_e$ (0.3987) at 2 g indicates closer agreement between predicted and experimental adsorption, while the highest $F_e$ (2.0108) at 10 g demonstrates substantial deviation, highlighting that the model underestimates adsorption capacity at higher adsorbent masses. Overall, these results suggest that the Boyd kinetic model does not consistently describe phosphorus adsorption onto raw Lala clam shells, making it less reliable than pseudo-first and pseudo-second order models for raw Lala clam shells.

Comparatively, Bektaş et al. (2021) investigated the diffusion mechanisms of phosphorus sorption using Boyd's internal and external diffusion models, revealing that both external and internal diffusion significantly influence the adsorption process. Their findings showed that the Boyd external diffusion model exhibited strong correlations, with $R^2$ values ranging from 0.88 to 0.99. However, in contrast to this study, the adsorption exhibited weak correlations with Boyd's kinetic model, with the highest adsorption capacity (6 g of adsorbent) showing an $R^2$ of only 0.4316. This trend suggests that film diffusion was not the primary rate-controlling step. Additionally, the results of Boyd's kinetic model from this study indicated that increasing adsorbent mass did not necessarily enhance adsorption efficiency, as particle aggregation at higher masses reduced the available surface area for adsorption.

Comparatively, Bektaş et al. (2021) investigated phosphate sorption mechanisms using Boyd's internal and external diffusion models. Strong correlations were reported for both models, with $R^2$ values ranging from 0.88 to 0.99, indicating that both film diffusion and intraparticle diffusion contributed significantly to the overall sorption process onto ion-exchange resin. In contrast, this study shows weak correlations with the Boyd kinetic model across all adsorbent masses, with the highest $R^2$ value reaching only 0.4316 at 6 g. This substantial difference suggests that diffusion processes are not the dominant rate-controlling mechanisms for phosphorus adsorption onto raw Lala clam shells. Furthermore, variations in adsorbent mass did not lead to systematic improvements in Boyd model fitting, indicating that increasing adsorbent dosage did not enhance diffusion-controlled kinetics. This contrast highlights that diffusion mechanisms described by the Boyd model are highly dependent on adsorbent material and system characteristics.

According to the data obtained in this study, phosphorus adsorption onto raw Lala clam shells is best described by the pseudo-second order model compared to the pseudo-first order and Boyd kinetic models. This is evident as the highest $R^2$ value of the pseudo-second order model (0.9964) surpasses that of the pseudo-first order (0.6732) and Boyd (0.4316) models. In contrast, the lowest $F_e$ value of the pseudo-second order model (0.0324) is lower than that of the pseudo-first order (1.6242) and Boyd (0.3987) models. This indicates that phosphorus adsorption involves chemisorption, involving chemical interactions between phosphorus and the active sites of raw Lala clam shells (Manna et al., 2022).

## ISOTHERM ADSORPTION ONTO RAW LALA CLAM SHELL THROUGH SOLUTIONS

The Isotherm adsorption model was applied by using Langmuir, Freundlich, and Henry's models to define a relationship between the presence of adsorbate quantities on the raw Lala clam shells and the characteristics of metal ions between solid and liquid forms (Abdullah et al., 2023). Figure 8 depicts the plot of (a) Freundlich model of ln ($C_e$) against ln ($q_e$), (b) Langmuir model of 1/ $q_e$ against 1/ $C_e$, and (c) Henry's isotherm model of $q_e$ against $C_e$.

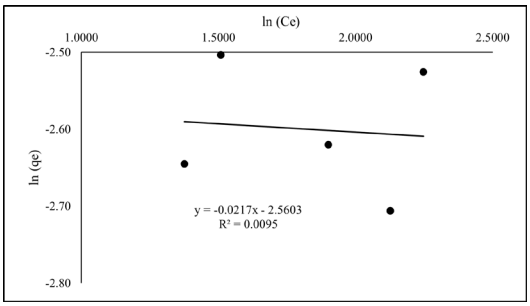


(a)

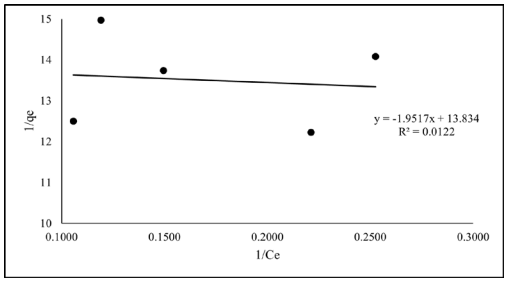


(b)

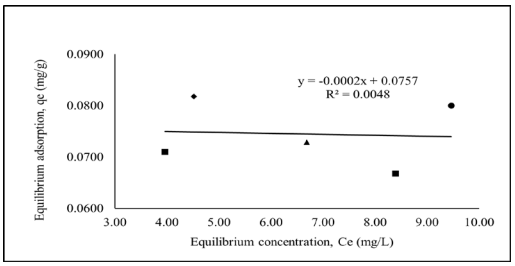


(c)

FIGURE 8. Isotherm models; (a) Freundlich model of ln ($C_e$) against ln ($q_e$), (b) Langmuir model of 1/ $q_e$ against 1/ $C_e$, and (c) Henry's isotherm model of $q_e$ against $C_e$

Table 4 summarizes the parameters obtained for each model, including the correlation coefficient ($R^2$), which indicates the goodness of fit of the models to the experimental data. As with the kinetic adsorption models, a higher $R^2$ value indicates a better fit of the model to the experimental data.

TABLE 4. Isotherm parameters for (a) Freundlich, (b) Langmuir, and (c) Henry's model parameters

| (a) Freundlich model parameters | | |
|---|---|---|
| n | $K_f$ (mg/g) | $R^2$ |
| 46.0829 | 0.0773 | 0.0095 |
| (b) Langmuir model parameters | | |
| q max (mg/g) | $K_L$ (L/mg) | $R^2$ |
| 0.0723 | -7.0882 | 0.0122 |
| (c) Henry's isotherm model parameters | | |
| $K_H$ (L/g) | $R^2$ | |
| -0.0002 | 0.0048 | |

Based on Table 4(a), the Freundlich model exhibits a very low $R^2$ value of 0.0095, indicating a poor fit to the adsorption process. This suggests that phosphorus adsorption onto the Lala clam shell does not predominantly occur on heterogeneous surfaces or involve multilayer adsorption (Kumari & Dong, 2025). Conversely, Nayeem et al. (2023) reported a strong correlation for phosphorus adsorption onto cockle shells using the Freundlich model ($R^2$ = 0.9836), suggesting a significantly different adsorption behavior. Abdullah et al. (2023a) observed a moderate fit to the Freundlich model ($R^2$ = 0.8418) for ore waste, indicating heterogeneous adsorption with chemical interactions. However, in this study, the Freundlich constant (n = 46.0829) for phosphorus adsorption onto raw Lala clam shells is exceptionally high, suggesting weak interactions between phosphate ions and the adsorbent, which results in inefficient adsorption (Amare et al., 2025). In comparison, Muslim et al. (2025) reported a Freundlich n-value of -4.9701 for marsh clam shell adsorption, which is significantly lower, indicating a different adsorption mechanism.

As can be seen in Table 4, among the three models, the Langmuir model in this study provides the highest $R^2$ value (0.0122), suggesting a slightly better fit than the Freundlich and Henry models. The results imply that phosphorus adsorption occurs as a monolayer on a surface with finite, identical adsorption sites (Vagi et al., 2025). However, the negative Langmuir constant ($K_L$ = -7.0882) indicates an energetically unfavorable adsorption process, likely due to weak bonding interactions between phosphorus and the adsorbent surface (Ganta et al., 2021). Nayeem et al. (2023) found a much higher $R^2$ value of 0.9681 for the Langmuir model when using cockle shell powder as an adsorbent, suggesting that phosphorus adsorption onto cockle shells primarily occurs through monolayer adsorption. Similarly, Muslim et al. (2025) reported that phosphorus adsorption onto marsh clam shells was better described by the Langmuir model ($R^2$ = 0.9392), with a maximum adsorption capacity ($q_{max}$) value of 0.1603 mg/g. Abdullah et al. (2023a) found that ore waste

adsorption fit the Langmuir model with the $R^2$ value of 0.827, showing moderate adsorption behavior, though still significantly higher than the Lala clam shell results.

According to Table 4(c), the Henry's isotherm model results in this study exhibit the lowest $R^2$ value of 0.0048 and a negative $K_H$ value (-0.0002 L/g), indicating that phosphorus adsorption onto Lala clam shells does not follow a simple linear relationship (Vagi et al., 2025). A negative KH value typically implies unfavorable adsorption conditions, possibly due to weak adsorbate-adsorbent interactions or desorption at higher concentrations (Ragaditha & Nandiyanto, 2021). In comparison, Silva et al. (2025) reported a significantly better fit for the Henry model in their study on phosphorus adsorption using functionalized mesoporous silica, with an $R^2$ value of 0.995. This suggests that Henry's model can accurately describe adsorption behavior for certain adsorbents, unlike the poor fit observed for Lala clam shells in this study.

In this study, the Langmuir model provides the best fit among the three, indicating that adsorption occurs through monolayer formation on a homogeneous surface (Vagi et al., 2025). However, the negative Langmuir constant and low adsorption capacity suggest limitations in adsorption efficiency, implying that surface modifications or alternative adsorbents may be needed to enhance phosphorus removal (Ganta et al., 2021). The Langmuir model predicts that phosphorus adsorption occurs at a finite number of uniform sites on the Lala clam shell surface, with each site can hold only one phosphorus molecule. Once occupied, no further adsorption can take place, reinforcing the monolayer adsorption mechanism (Ragaditha & Nandiyanto, 2021).

## CONTOUR PREDICTION OF PHOSPHORUS REMOVAL EFFICIENCY AND REQUIRED MASS ADSORBENT ONTO RAW LALA CLAM SHELL

A contour diagram would be helpful in instantly determining the removal efficiency trend (Abdullah et al., 2023). This analysis delivers a greater understanding of the relationship between initial adsorption situations and removal efficiency, as depicted in Figure 10.

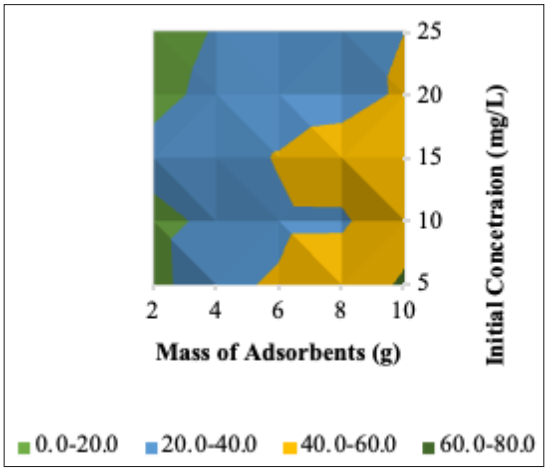


FIGURE 10. Contour prediction diagram of phosphorus removal efficiency for raw Lala clam shell

Figure 10 illustrates the relationship between phosphorus removal efficiency and two independent variables, the initial phosphorus concentration and the adsorbent mass. This contour diagram provides insights into the adsorption behavior under varying conditions. For instance, when the initial phosphorus concentration is 20 mg/L, an adsorbent mass of 6 g achieves an estimated removal efficiency between 40% and 60%.

The results of this study align with findings from previous research. Muslim et al. (2025) reported that a similar initial phosphorus concentration of 20 mg/L achieved a removal efficiency of 20% to 40% using 6 g of marsh clam shell. Additionally, Abdullah et al. (2023) indicated that 7.5 g of ore waste removed 30% to 40% of phosphorus from an aqueous solution with an initial concentration of 20 mg/L. In contrast, 5.2 g of ore waste removed 10% to 20% of phosphorus at an initial concentration of 12.5 mg/L. In comparison, 3.5 g of ore waste removed a similar percentage when the initial concentration was 15 mg/L.

This contour diagram shows that the necessary adsorbent mass can be estimated to achieve the desired removal efficiency. Even though more precise values could be calculated using the developed equations, this contour prediction diagram provides a practical way to observe trends in removal efficiency as a function of initial adsorption conditions immediately. This allows for a quick assessment of the relationship between phosphorus removal and adsorption conditions (Zaini et al., 2025).

## CONCLUSION

In conclusion, the objectives of this study which is to elucidate the physicochemical characteristics of raw Lala clam shells as adsorbents, to determine the removal efficiency, E (%), and adsorption capacity, q (mg/g), of raw Lala clam shells for phosphorus removal from aqueous phosphate solutions at equilibrium, to assess the kinetic and isotherm adsorption models governing phosphorus removal, and to evaluate the effectiveness of phosphorus removal at varying adsorbent masses and initial concentrations using a contour prediction diagram, have been successfully achieved.

Physicochemical characterization confirmed that raw Lala clam shells are predominantly composed of aragonite-type calcium carbonate, as demonstrated by XRD analysis. The aragonite crystalline structure remained intact after phosphorus adsorption, indicating that adsorption occurred mainly on the surface without altering the fundamental $CaCO_3$ framework. The absence of detectable crystalline phosphorus phases after adsorption suggests that phosphorus was likely present as amorphous or highly dispersed calcium phosphate species on the shell surface, consistent with adsorption–precipitation mechanisms reported for biogenic calcium carbonate materials. SEM observations further supported successful phosphorus uptake, revealing a transformation from a porous, rough surface to a denser and more compact morphology after adsorption, with pore blockage and particle aggregation indicative of phosphate attachment. EDXRF and FTIR analyses confirmed chemical interactions between phosphorus and calcium-rich components, as well as the involvement of hydroxyl and nitrogen-containing functional groups, while preserving the core carbonate structure of the shells.

Batch adsorption experiments demonstrated that phosphorus removal efficiency increased with increasing adsorbent mass, reaching a maximum removal efficiency of 64.20% at an adsorbent mass of 10 g, with equilibrium attained at 1440 min. The adsorption capacity ranged from 0.0668 to 0.0818 mg/g, with the highest capacity observed at an adsorbent mass of 8 g. Although adsorption capacity did not increase proportionally with adsorbent mass due to saturation of active sites and reduced solute availability, these results confirm that raw Lala clam shells are capable of measurable phosphorus uptake despite being used in an untreated form. Kinetic analysis revealed that the pseudo-second order model best described the adsorption process, exhibiting the highest correlation coefficient ($R^2 = 0.9964$) and the lowest error function value ($F_e = 0.0324$) compared to the pseudo-first order and Boyd models. This indicates that phosphorus adsorption onto raw Lala clam shells is primarily governed by chemisorption involving chemical interactions between phosphate ions and active surface sites, rather than being controlled by film diffusion mechanisms. The poor fit of the Boyd model further confirms that diffusion is not the dominant rate-controlling step in this system.

Isotherm analysis showed generally low correlation coefficients for all three models investigated. Among them, the Langmuir model provided the relatively best fit, suggesting monolayer adsorption on a homogeneous surface with finite adsorption sites. However, the negative Langmuir constant and very low $R^2$ values indicate energetically unfavorable adsorption and weak adsorbate–adsorbent interactions, highlighting the limited adsorption efficiency of raw Lala clam shells. Freundlich and Henry's models exhibited poorer fits, confirming that phosphorus adsorption onto raw Lala clam shells does not follow multilayer or linear adsorption behavior under the studied conditions.

The contour prediction diagram successfully illustrated the combined effects of adsorbent mass and initial phosphorus concentration on removal efficiency, providing a practical tool for estimating the required adsorbent dosage to achieve targeted removal levels. This approach enables rapid visualization of adsorption trends and supports decision-making for process optimization without extensive experimental repetition.

Overall, raw Lala clam shells exhibited moderate adsorption performance, which is consistent with their application in an untreated, unmodified form. Despite the relatively low adsorption capacity, the results confirm measurable phosphorus uptake and highlight the potential applicability of shell waste as a low-cost and sustainable adsorbent, particularly for preliminary or supplementary phosphorus removal. Future studies should focus on surface modification strategies, regeneration and reuse potential, and evaluation under real wastewater conditions to further enhance adsorption performance and assess large-scale applicability.

## ACKNOWLEDGEMENT

This research was supported by Universiti Tun Hussein Onn Malaysia (UTHM) through a Multidisciplinary Research Grant (MDR) Vot Q744 and GPPS (Vot Q673).

## DECLARATION OF COMPETING INTEREST

None.

## REFERENCES


Abdullah, N. H., Adnan, N. A., Mohd Rashidi, N. F. N., Yaacob, M. S. S. & Abdul Salim, N. A. 2022a. Comparing the adsorption isotherms and kinetics of phosphate adsorption on various waste shells as adsorbent. *Water Practice & Technology* 17(5): 974–985.

Abdullah, N. H., Hasan, H., Razani, M. A. D., Hassan, M. H. I., Yaacob, M. S. S., Salim, N. A. A. et al. 2022b. Phosphorus Removal from Aqueous Solution by Using Calcined Waste Chicken Eggshell: Kinetic and Isotherm Model.

Abdullah, N. H., Nizam, W. H. A., Norhisham, M. H. I., Husaimi, N. A., Ngadiman, N., Salim, N. A. A. et al. 2023a. Phosphorus removal from ore waste in aqueous solution with different mass of ore waste adsorbent from the Johor mine site. *Water Practice & Technology* 18(11): 2957–2970.

Abdullah, N. H., Shanmuganathan, R., Muthusamy, T., Zi, Y. & Jusoh, N. H. 2024. Phosphate adsorption from aqueous solution using different mass of raw waste marsh clam shells as an alternative novel adsorber.

Abdullah, N. H., Xian, O. J., Yi, C. Z., Yuan, N. S., Yaacob, M. S. S., Salim, N. A. A. & Abdullah, F. 2023b. Removal of phosphate from synthetic wastewater by using marsh clam (Polymesoda expansa) shell as an adsorbent. *Biointerface Research in Applied Chemistry* 13(1): 56.

Adly, A., Mostafa, N. G. & Elawwad, A. 2022. Adsorption of phosphorus onto nanoscale zero-valent iron/activated carbon: removal mechanisms, thermodynamics, and interferences. *Water Reuse* 12(1): 111–130.

Ahmed Eljiedi, A. A., Kamari, A., Sunardi & Fatimah, I. 2019. Lala clam (Orbicularia orbiculata) shell as an eco-friendly adsorbent for Cd (II), Cu (II) and Pb (II) ions. *Arab Journal of Basic and Applied Sciences* 26(1): 462–475.

Ai, D., Ma, H., Meng, Y., Wei, T. & Wang, B. 2023. Phosphorus recovery and reuse in water bodies with simple ball-milled Ca-loaded biochar. *Science of the Total Environment* 860: 160502.

Akinnawo, S. O. 2023. Eutrophication: Causes, consequences, physical, chemical and biological techniques for mitigation strategies. *Environmental Challenges* 12: 100733.

Albetran, H. M. 2020. Structural characterization of graphite nanoplatelets synthesized from graphite flakes.

Ali, A., Chiang, Y. W. & Santos, R. M. 2022. X-ray diffraction techniques for mineral characterization: A review for engineers of the fundamentals, applications, and research directions. *Minerals* 12(2): 205.

Ali, M. A., Chambers, C., Reza, M. T. & Aich, N. 2024. Application of corn stover derived pyrolyzed hydrochars for efficient phosphorus removal from water: Influence of pyrolysis temperature. *Chemical Engineering Journal Advances* 18: 100613.

Amare, A., Kassa, Y., Lemma, B., Bhaskarwar, A. N., Mullu, T. & Tibebe, D. 2025. Optimised phosphate adsorption using a synergistic calcite-dolomite mix: a novel approach for water treatment. *Chemistry and Ecology* 1-26.

Azarian, M. H. & Sutapun, W. 2022. Biogenic calcium carbonate derived from waste shells for advanced material applications: A review. *Frontiers in Materials* 9: 1024977.

Bashir, M., Batool, M., Arif, N., Tayyab, M., Zeng, Y. J. & Zafar, M. N. 2023. Strontium-based nanomaterials for the removal of organic/inorganic contaminants from water: A review. *Coordination Chemistry Reviews* 492: 215286.

Benaoune, S., Merzougui, A., Remmani, R., Bouzidi, N., Ruiz-Canales, A., Akacha, I. & Djellouli, A. 2025. Dual-Activated Tamarix Gallica-Derived Carbons for Enhanced Glyphosate Adsorption: A Comparative Study of Phosphoric and Sulfuric Acid Activation. *Materials* 18(3): 511.

Benjelloun, M., Miyah, Y., Evrendilek, G. A., Zerrouq, F. & Lairini, S. 2021. Recent advances in adsorption kinetic models: their application to dye types. *Arabian Journal of Chemistry* 14(4): 103031.

Brakemi, E., Michael, K., Tan, S. P. & Helen, H. 2023. Phosphate removal from wastewater using scallop and whelk shells. *Journal of Water Process Engineering* 55: 104159.

Brandão, P., Marques, C. S., Carreiro, E. P., Pineiro, M. & Burke, A. J. 2021. Engaging isatins in multicomponent reactions (MCRs)–easy access to structural diversity. *The Chemical Record* 21(4): 924–1037.

Cao, Q. N., Cherqaoui, A., Henrique Michelin Beraldo, C., Paternoster, C., Gélinas, S., Blais, C. et al. 2025. Effect of Volumetric Energy Density on the Evolution of the Microstructure and the Degradation Behavior of 3D-Printed Fe-Mn-C Alloys from Water-Atomized Powders. *Metals* 15(2): 101.

Chae, S., Murugesan, B., Kim, H., Duvvuru, D. K., Lee, T., Choi, Y. H. et al. 2021. Advanced phosphorus recovery from municipal wastewater using anoxic/aerobic membrane bioreactors and magnesium carbonate-based pellets. *ACS ES&T Water* 1(8): 1657–1664.

Chen, P., Chen, D., Zhao, W. & Zheng, X. 2022. Aeration Biofilter Filler Screening and Experimental Research on Nitrogen and Phosphorus Purification in Rural Black Water. *Water* 14(6): 957.

Chen, Z. G., Li, S. M., Chen, J., Wan, H. Y., Lin, W. X., Wang, M. & Du, J. D. 2023. The effects of phosphate concentration on the recovery of phosphate from alkaline solution by hydrated lime and calcined oyster shell: recovery efficiency, capacity and

hydroxyapatite purity. *Environmental Advances* 12: 100363.

Deng, P., Karadge, M., Rebak, R. B., Gupta, V. K., Prorok, B. C. & Lou, X. 2020. The origin and formation of oxygen inclusions in austenitic stainless steels manufactured by laser powder bed fusion. *Additive Manufacturing* 35: 101334.

Ehiomogue, P., Ahuchaogu, I. I. & Ahaneku, I. E. 2021. Review of adsorption isotherms models. *Acta Technica Corviniensis-Bulletin of Engineering* 14(4).

Ganta, P. B., Morshedizad, M., Kühn, O., Leinweber, P. & Ahmed, A. A. 2021. The binding of phosphorus species at goethite: A joint experimental and theoretical study. *Minerals* 11(3): 323.

Gokila, A. & Ayyappan, S. 2021. Quantum chemical insight properties of glyphosine (N, N-Bis (phosphonomethyl) glycine)–a combined hf and density functional study. *Digest Journal of Nanomaterials & Biostructures (DJNB)* 16(2).

Habte, L., Khan, M. D., Shiferaw, N., Farooq, A., Lee, M. H., Jung, S. H. & Ahn, J. W. 2020. Synthesis, characterization and mechanism study of green aragonite crystals from waste biomaterials as calcium supplement. *Sustainability* 12(12): 5062.

Hamid, M. S. 2022. Effect of Sea-shell Based Calcium Carbonate Supplement (Cockle) on the Egg Quality of Japanese Quail (Coturnix coturnix japonica). Doctoral dissertation, , Chittagong Veterinary and Animal Sciences University Chittagong–4225, Bangladesh.

Ikhsan, N., Sekewael, S. J. & Hasanela, N. 2022. Kinetics and isotherm study of ion phosphate adsorption by Lontor natural clay. *Indonesian Journal of Chemical Research* 9(3): 171–178.

Kazak, A., Simonov, K. & Kulikov, V. 2021. Machine-learning-assisted segmentation of focused ion beam-scanning electron microscopy images with artifacts for improved void-space characterization of tight reservoir rocks. *SPE Journal* 26(04): 1739–1758.

Kesari, K. K., Soni, R., Jamal, Q. M. S., Tripathi, P., Lal, J. A., Jha, N. K. et al. 2021. Wastewater treatment and reuse: a review of its applications and health implications. *Water, Air, & Soil Pollution* 232: 1–28.

Khalil, K. D., Riyadh, S. M., Alkayal, N. S., Bashal, A. H., Alharbi, K. H. & Alharbi, W. 2022. Chitosan-strontium oxide nanocomposite: preparation, characterization, and catalytic potency in thiadiazoles synthesis. *Polymers* 14(14): 2827.

Khan, M. D., Chottitisupawong, T., Vu, H. H., Ahn, J. W. & Kim, G. M. 2020. Removal of phosphorus from an aqueous solution by nanocalcium hydroxide derived from waste bivalve seashells: mechanism and kinetics. *ACS omega* 5(21): 12290–12301.

Kljajević, L., Nenadović, M., Ivanović, M., Bučevac, D., Mirković, M., Mladenović Nikolić, N. & Nenadović, S. 2022. Heat treatment of geopolymer samples obtained by varying concentration of sodium hydroxide as constituent of alkali activator. *Gels* 8(6): 333.

Kumari, S. & Dong, Y. 2025. Alcan-based adsorption: Mitigating phosphate pollution in subsurface drainage water. *Journal of Water Process Engineering* 69: 106781.

Lee, J. I., Kang, J. K., Oh, J. S., Yoo, S. C., Lee, C. G., Jho, E. H. & Park, S. J. 2021. New insight to the use of oyster shell for removing phosphorus from aqueous solutions and fertilizing rice growth. *Journal of Cleaner Production* 328: 129536.

Li, C., Shen, H., Sheng, X., Wei, H. & Chen, J. 2020. Kinetics and fractionation of carbon and oxygen isotopes during the solid-phase transformation of biogenic aragonite to calcite: The effect of organic matter. *Palaeogeography, Palaeoclimatology, Palaeoecology* 556: 109876.

Li, X., Lv, G., Ma, W., Li, T., Zhang, R., Zhang, J. et al. 2022. Review of resource and recycling of silicon powder from diamond-wire sawing silicon waste. *Journal of Hazardous Materials* 424: 127389.

Li, Y., Nan, X., Li, D., Wang, L., Xu, R. & Li, Q. 2021. Advances in the treatment of phosphorus-containing wastewater. In *IOP Conference Series: Earth and Environmental Science 647(1): 012163*. IOP Publishing.

Longhini, C. M., Mahieu, L., Sá, F., van den Berg, C. M., Salaün, P. & Neto, R. R. 2021. Coastal waters contamination by mining tailings: What triggers the stability of iron in the dissolved and soluble fractions? Limnology and Oceanography, 66(1), 171-187.

Maimulyanti, A., Nurhidayati, I. & Widarsih, R. W. 2022. Adsorption isotherm models and kinetics for phosphate adsorption in sediment. *Rasayan Journal of Chemistry* 15(4).

Manna, A., Naskar, N., Sen, K. & Banerjee, K. 2022. A review on adsorption mediated phosphate removal and recovery by biomatrices. *Journal of the Indian Chemical Society* 99(10): 100682.

María Lorena, C. A., Verónica Cristina, A. Y., Alda, G. L., Ronald Oswaldo, V. T., Lorena, C. C. R., Sarah, A. C. T. et al. 2025. Use of Modified Activated Carbon in Groundwater Remediation for Human Consumption. *Water* 17(2): 207.

Masliha, M., Padnekar, M., De Micco, J., Ponnupandian, S., Mondal, K. & Padamati, R. B. 2025. Functionalized Organosolv Lignin Grafted with 3-Aminopropyltriethoxysilane: A Bio-based Adsorbent for Phosphate Recovery from Dairy Wastewater. *Heliyon*.

Massit, A., El Yacoubi, A., Kholtei, A. & El Idrissi, B. C. 2021. XRD and FTIR analysis of magnesium substituted tricalcium calcium phosphate using a wet precipitation method. *Biointerface Res. Appl. Chem* 11(1): 8034–8042.

Medel, R. & Suhm, M. A. 2021. Predicting OH stretching fundamental wavenumbers of alcohols

for conformational assignment: Different correction patterns for density functional and wave-function-based methods. *Physical Chemistry Chemical Physics* 23(9): 5629–5643.

Mititelu, M., Stanciu, G., Drăgănescu, D., Ioniță, A. C., Neacșu, S. M., Dinu, M. et al. 2021. Mussel shells, a valuable calcium resource for the pharmaceutical industry. *Marine Drugs* 20(1): 25.

Mohamed, N. B., Ngadi, N., Yahya, N. Y., Mohamed Noor, M. H., Bakar, A. A. & Ali, N. 2025. Optimization Study of Ammonium Adsorption from Aqueous Solution on Carbon Black Modified with Sodium Dodecylbenzene Sulfonate: Kinetics, Isotherms, and Thermodynamics. *Arabian Journal for Science and Engineering* 1-22.

Mohan, V., Naske, C. D., Britten, C. N., Karimi, L. & Walters, K. B. 2020. Hydroxide-catalyzed cleavage of selective ester bonds in phosphatidylcholine: An FTIR study. *Vibrational Spectroscopy* 109: 103055.

Mokhtera, M. A., binti Azmi, N. N. & Wena, L. W. 2023. Removal of Cadmium from Water by using Clam Shell-Based Membrane Through Adsorption.

Moustafa, H., Shemis, M. A., Ahmed, E. M. & Isawi, H. 2024. Improvement of hybrid polyvinyl chloride/dapsone membrane using synthesized silver nanoparticles for the efficient removal of heavy metals, microorganisms, and phosphate and nitrate compounds from polluted water. *RSC advances* 14(28): 19680–19700.

Mphahlele, M. R., Mosai, A. K., Tutu, H. & Kotzé, I. A. 2025. Enhanced platinum and palladium recovery from aqueous solutions: a comparative study of acylthiourea and amine-modified silica gel adsorbents. *RSC advances* 15(6): 4607–4618.

Muchunku, E. M., Ndiba, P. K. & Omondi, E. A. 2023. Defluoridation of Groundwater by Activated Carbon Derived from Water Hyacinth (Pontederia crassipes) by Phosphoric Acid Activation. *American Journal of Water Science and Engineering* 9(4): 97–107.

Muslim, N. H., Faizal, A. D. M., Sophian, M. A. S., Abd Rashid, M. A. F., Abdullah, N. H., Hassan, N. A. & Salim, N. A. A. 2025. Removal of Phosphorus from Water onto Marsh Clam Shell to Predict Contour for Removal Efficiency and Mass of Adsorbent. *Jurnal Kejuruteraan* 37(1): 309–321.

Nandiyanto, A. B. D., Nur, N. & Taufik, R. S. R. 2022. Investigation of adsorption performance of calcium carbonate microparticles prepared from eggshells waste. *Journal of Engineering Science and Technology* 17(3): 1934–1943.

Nguyen, Q. H., Ly, H. B., Ho, L. S., Al-Ansari, N., Le, H. V., Tran, V. Q. et al. 2021. Influence of data splitting on performance of machine learning models in prediction of shear strength of soil. *Mathematical Problems in Engineering* 2021(1): 4832864.

Nhung, N. T. H., Long, V. D. & Fujita, T. 2023. A Critical Review of Snail Shell Material Modification for Applications in Wastewater Treatment. *Materials* 16(3): 1095.

Owhonka, A., Fubara, E. F. & Justice, O. B. 2021. Wastewater quality-it's impact on the environment and human physiology: a Review. *Int. J. Adv. Res. Innov* 9: 43–58.

Park, J. H., Yang, J., Kim, D., Gim, H., Choi, W. Y. & Lee, J. W. 2022. Review of recent technologies for transforming carbon dioxide to carbon materials. *Chemical Engineering Journal* 427: 130980.

Pervov, A., Aung, H. Z. & Spitsov, D. 2023. Treatment of mine water with reverse osmosis and concentrate processing to recover copper and deposit calcium carbonate. *Membranes* 13(2): 153.

Piaskowski, K. & Zarzycki, P. K. 2020. Carbon-based nanomaterials as promising material for wastewater treatment processes. *International Journal of Environmental Research and Public Health* 17(16): 5862.

Pikula, K., Chaika, V., Zakharenko, A., Savelyeva, A., Kirsanova, I., Anisimova, A. & Golokhvast, K. 2020. Toxicity of carbon, silicon, and metal-based nanoparticles to the hemocytes of three marine bivalves. *Animals* 10(5): 827.

Rebora, M., Salerno, G., Piersanti, S., Saitta, V., Morelli Venturi, D., Li, C. & Gorb, S. 2023. The armoured cuticle of the black soldier fly Hermetia illucens. *Scientific Reports* 13(1): 22101.

Saleh, A. A. S., Ibrahim, N., Awang, N. R., & Akbar, N. A. (2021, August). Characteristics study of ammonia-n and phosphorus in sewage wastewater effluent: a case study of Alkhumrah, Jeddah Wastewater Treatment Plant. In IOP Conference Series: Earth and Environmental Science (Vol. 842, No. 1, p. 012034). IOP Publishing.

Saleh, T. A. 2022. Kinetic models and thermodynamics of adsorption processes: Classification. In *Interface science and technology 34: 65–97*. Elsevier.

Salim, N. A. A., Puteh, M. H., Khamidun, M. H., Fulazzaky, M. A., Abdullah, N. H., Yusoff, A. R. M. et al. 2021. Interpretation of isotherm models for adsorption of ammonium onto granular activated carbon. *Biointerface Res. Appl. Chem* 11(2): 9227–9241.

Schöne, B. R., Marali, S., Jantschke, A., Mertz-Kraus, R., Butler, P. G. & Fröhlich, L. 2023. Can element chemical impurities in aragonitic shells of marine bivalves serve as proxies for environmental variability? Chemical Geology, 616, 121215.

Shao, Y., Li, J., Fang, X., Yang, Z., Qu, Y., Yang, M. et al. 2022. Chemical modification of bamboo activated carbon surface and its adsorption property of simultaneous removal of phosphate and nitrate. *Chemosphere* 287: 132118.

Sheng, X., Chen, S., Zhao, Z., Li, L., Zou, Y., Shi, H. et al. 2023. Rationally designed calcium carbonate multifunctional trap for contaminants adsorption. *Science of The Total Environment* 166142.

Shi, L., Zhao, X., Cao, Y., Ma, H. & Sun, X. 2023. Physicochemical properties and phosphorus adsorption capacity of ceramsite made from alum sludge. *Water* 15(13): 2427.

Shukhairi, S. S., Mazlan, N., Subbiah, V. K., Abd Rahman, N. N., Nazahuddin, M. N. A., Shawel, A. S. et al. 2025. Evaluation of Microplastics Ingested by Sea Cucumber Holothuria Scabra from Pulau Jambongan, Sabah. *Bulletin of Environmental Contamination and Toxicology* 114(1): 1–9.

Silva, J. A. 2023. Wastewater treatment and reuse for sustainable water resources management: a systematic literature review. *Sustainability* 15(14): 10940.

Singh, A., Himanshu, M., Verma, B., Singh, R., Lal, B., Syed, A. et al. 2025. Evaluation of sustainability of fabrication process and characterization studies of activated carbon nanocatalyst from waste chestnut peels. *Journal of Molecular Structure* 1321: 139810.

Singh, S., Naik, T. S. K., Anil, A. G., Khasnabis, S., Nath, B., Basavaraju, U. et al. 2022. A novel CaO nanocomposite cross linked graphene oxide for Cr (VI) removal and sensing from wastewater. *Chemosphere* 301: 134714.

Sun, J., Zhu, W., Cao, J., Zhong, J., Mu, B., Wang, X. & Lin, N. 2023. Improving the yield and tetracycline adsorption performance of kitchen waste biochar through subcritical dimethyl ether pretreatment. *Journal of Environmental Chemical Engineering* 11(5): 110459.

Svedaite, E., Dambrauskas, T., Renman, A., Renman, G. & Baltakys, K. 2025. Adsorption kinetics of phosphorus on a calcium silicate hydrate based adsorbent. *Ceramics International* 51(5): 5557–5566.

Swapna, M. S. & Sankararaman, S. 2020. Organometallic sodium carbide for heat transfer applications: a thermal lens study. *International Journal of Thermophysics* 41(7): 93.

Tian, H., Guo, Z., Pan, J., Zhu, D., Yang, C., Xue, Y. et al. 2021. Comprehensive review on metallurgical recycling and cleaning of copper slag. *Resources, Conservation and Recycling* 168: 105366.

Tong, H., Wang, W., Wang, G., Wang, X., Yu, D., Chen, B. & Pei, K. 2024. Synthesis and characterization of non-ionic flame-retardant waterborne polyurethane. *RSC advances* 14(44): 32031–32040.

Ubaldini, A., Cicconi, F., Calistri, S., Salvi, S., Telloli, C., Marghella, G. et al. 2024. Removal of Organic Materials from Mytilus Shells and Their Morphological and Chemical-Physical Characterisation. *Crystals* 14(5): 464.

Usman, M. O., Aturagaba, G., Ntale, M. & Nyakairu, G. W. 2022. A review of adsorption techniques for removal of phosphates from wastewater. *Water Science & Technology* 86(12): 3113–3132.

Vagi, M. C., Petsas, A. S., Dimitropoulou, D., Leventelli, M. & Nikolaou, A. D. 2025. Adsorption of Methylene Blue Dye onto Various Marine Sediments and Seagrass Biomass of Posidonia oceanica Species: Kinetics and Equilibrium Studies.

Verma, A. K., Rahman, A., Hussain, S. & Singh, N. S. 2025. Freshwater Mussels as Multifaceted Ecosystem Engineers: Insights into Their Ecological Importance, Bioindication, and Economic Contributions.

Verma, S., Kim, K. H., Kumar, N., Bhattacharya, S. S., Naushad, M. & Dutta, R. K. 2022. Amine-amide functionalized graphene oxide sheets as bifunctional adsorbent for the removal of polar organic pollutants. *Journal of Hazardous Materials* 429: 128308.

Wang, L., Li, H., Dong, H., Cheng, Y., He, W. & Xu, Y. 2025. Efficient phosphorus removal using the La-based perovskite oxides: Role of B-site metal for modulating the surface electronic structure. *Environmental Engineering Research* 30(2): 192–207.

Witek-Krowiak, A., Gorazda, K., Szopa, D., Trzaska, K., Moustakas, K. & Chojnacka, K. 2022. Phosphorus recovery from wastewater and bio-based waste: an overview. *Bioengineered* 13(5): 13474–13506.

Yadav, V. K., Yadav, K. K., Cabral-Pinto, M. M., Choudhary, N., Gnanamoorthy, G., Tirth, V. et al. 2021. The processing of calcium rich agricultural and industrial waste for recovery of calcium carbonate and calcium oxide and their application for environmental cleanup: A review. *Applied Sciences* 11(9): 4212.

Yang, C. (2022, December). Review on the causes of eutrophication in water. In 2022 6th International Seminar on Education, Management and Social Sciences (ISEMSS 2022) (pp. 246-252). Atlantis Press.

Yang, H., Zhang, H., Lu, J., Cui, Y., Wang, Y., Wang, X. et al. 2025. Advanced magnetic adsorbents for enhanced phosphorus and fluoride removal from wastewater: Mechanistic insights and applications. *Separation and Purification Technology* 353: 128195.

Zaini, M. S. M., Roslan, S. Z., Za'aim, M. A. M. & Syed-Hassan, S. S. A. 2025. Optimization of the preparation of palm kernel shell–derived activated carbon via Taguchi method for enhanced methylene blue removal. *Biomass Conversion and Biorefinery* 1-17.

Zhang, J., Jin, X. & Yang, C. 2022. Efficient removal of organic pollutants in waste sulfuric acid by an advanced oxidation process using coconut shell-derived biochar to produce qualified poly aluminium sulfate. *Separation and Purification Technology* 293: 121057.

Zhang, L., Liu, Y., Wang, Y., Li, X. & Wang, Y. 2021. Investigation of phosphate removal mechanisms by a lanthanum hydroxide adsorbent using p-XRD, FTIR and XPS. *Applied Surface Science* 557: 149838.

Zheng, Z., Own, C. S., Wanner, A. A., Koene, R. A., Hammerschmith, E. W., Silversmith, W. M. et al. 2024. Fast imaging of millimeter-scale areas with beam deflection transmission electron microscopy. *Nature Communications* 15(1): 6860.

Zojaji, I., Esfandiarian, A. & Taheri-Shakib, J. 2021. Toward molecular characterization of asphaltene from different origins under different conditions by means of FT-IR spectroscopy. *Advances in Colloid and Interface Science* 289: 102314.